Total absorption γ-ray spectroscopy of the β-delayed neutron emitters ^{87}Br, ^{88}Br, and ^{94}Rb

E. Valencia, J. L. Tain,* A. Algora,† J. Agramunt, E. Estevez, M. D. Jordan, and B. Rubio
Instituto de Fisica Corpuscular (CSIC-Universitat de Valencia), Apartado de Correos 22085, E-46071 Valencia, Spain

S. Rice, P. Regan, W. Gelletly, Z. Podolyák, M. Bowry, P. Mason, and G. F. Farrelly
University of Surrey, Department of Physics, Guilford GU2 7XH, United Kingdom

A. Zakari-Issoufou, M. Fallot, A. Porta, and V. M. Bui
SUBATECH, CNRS/IN2P3, Universit de Nantes, Ecole des Mines, F-44307 Nantes, France

J. Rissanen, T. Eronen, I. Moore, H. Penttilä, J. Äystö, V.-V. Elomaa, J. Hakala, A. Jokinen, V. S. Kolhinen, M. Reponen, and V. Sonnenschein
University of Jyvaskyla, Department of Physics, P.O. Box 35, FI-40014 University of Jyvaskyla, Finland

D. Cano-Ott, A. R. Garcia, T. Martínez, and E. Mendoza
Centro de Investigaciones Energéticas Medioambientales y Tecnólogicas, E-28040 Madrid, Spain

R. Caballero-Folch, B. Gomez-Hornillos, and V. Gorlichev
Universitat Politecnica de Catalunya, E-08028 Barcelona, Spain

F. G. Kondev
Nuclear Engineering Division, Argonne National Laboratory, Argonne, Illinois 60439, USA

A. A. Sonzogni
NNDC, Brookhaven National Laboratory, Upton, New York 11973, USA

L. Batist
Petersburg Nuclear Physics Institute, Gatchina, Russia

(Received 20 September 2016; revised manuscript received 21 December 2016; published 21 February 2017)

We investigate the decay of ^{87,88}Br and ^{94}Rb using total absorption γ-ray spectroscopy. These important fission products are β-delayed neutron emitters. Our data show considerable $\beta\gamma$ intensity, so far unobserved in high-resolution γ-ray spectroscopy, from states at high excitation energy. We also find significant differences with the β intensity that can be deduced from existing measurements of the β spectrum. We evaluate the impact of the present data on reactor decay heat using summation calculations. Although the effect is relatively small it helps to reduce the discrepancy between calculations and integral measurements of the photon component for ^{235}U fission at cooling times in the range 1–100 s. We also use summation calculations to evaluate the impact of present data on reactor antineutrino spectra. We find a significant effect at antineutrino energies in the range of 5 to 9 MeV. In addition, we observe an unexpected strong probability for γ emission from neutron unbound states populated in the daughter nucleus. The γ branching is compared to Hauser-Feshbach calculations, which allow one to explain the large value for bromine isotopes as due to nuclear structure. However the branching for ^{94}Rb, although much smaller, hints of the need to increase the radiative width Γ_γ by one order of magnitude. This increase in Γ_γ would lead to a similar increase in the calculated (n,γ) cross section for this very neutron-rich nucleus with a potential impact on r process abundance calculations.

DOI: 10.1103/PhysRevC.95.024320

I. INTRODUCTION

Total absorption γ-ray spectroscopy (TAGS) has been applied to study the decay of three fission products (FP) which are β-delayed neutron emitters. We present in this work the results of this study and discuss the impact on three research topics of current interest: (1) reactor decay heat (DH) calculations, (2) reactor antineutrino $\bar{\nu}_e$ spectrum calculations, and (3) the study of the emission of γ rays from neutron-unbound states and its relation to neutron capture (n,γ) reactions.

The isotopes included in the present study are ^{87}Br, ^{88}Br, and ^{94}Rb. These are neutron-rich nuclei with relatively short half-life $T_{1/2}$, large decay energy window Q_β, large neutron separation energy S_n in the daughter nucleus, and moderate

*Corresponding author: tain@ific.uv.es
†Also at Institute of Nuclear Research of the Hungarian Academy of Sciences, H-4026 Debrecen, Hungary.

TABLE I. Half-life $T_{1/2}$, neutron emission probability P_n, decay energy window Q_β, and daughter neutron separation energy S_n for each measured isotope. Values taken from Refs. [1–3].

Isotope	$T_{1/2}$ (s)	P_n (%)	Q_β (MeV)	S_n (MeV)
^{87}Br	55.65(13)	2.60(4)	6.852(18)	5.515(1)
^{88}Br	16.34(8)	6.58(18)	8.975(4)	7.054(3)
^{94}Rb	2.702(5)	10.18(24)	10.281(8)	6.828(10)

neutron emission probability P_n as can be observed in Table I, showing decay parameters taken from the Evaluated Nuclear Structure Data File (ENSDF) [1–3].

The three aforementioned topics of research benefit from the application of the TAGS technique to obtain the β-intensity distribution of decays followed by γ-ray emission. States at high excitation energy in the daughter nucleus can be populated if Q_β is large. In this case both the number of levels over which the β intensity is distributed and the number of levels available for γ de-excitation is large. Thus individual γ rays collect little intensity and the use of high-resolution γ-ray spectroscopy (HRGS) with germanium detectors typically fails to detect some of them. This problem has come to be known as the *Pandemonium* effect [4]. As a consequence, β-intensity distributions determined from γ-ray intensity balance tend to be distorted with an excess of β intensity assigned at low excitation energies. The TAGS technique [5], using large 4π scintillation detectors, is based on the detection of the full de-excitation cascade, rather than individual γ rays, and thus overcomes the Pandemonium effect. The power of the TAGS method to locate the missing β intensity has been demonstrated before [6–8]. The distortion of the β-intensity distributions obtained from HRGS causes a systematic error in the calculated average β- and γ-decay energies. This affects the calculation of the DH time evolution using the summation method, which relies on decay data from individual precursors. Similarly, the distortion of the β intensity affects the calculated spectrum of antineutrinos emitted from reactors using the summation method. Pandemonium also prevents the correct determination of the γ-to-neutron emission ratios from states populated above S_n in the daughter nucleus.

Subsections I A, I B, and I C provide background information on the three research topics, detail the influence of Pandemonium for each of them, and points out the relevance of the selected isotopes. The remainder of the paper is organized as follows. Details of the experimental method are given in Sec. II. The analysis of the data, the β-intensity distributions, and the evaluation of uncertainties are presented in Sec. III. The impact of the average β- and γ-decay energies determined in this work on DH calculations is presented in Sec. IV. The effect on calculated antineutrino spectra is shown in Sec. V. The evaluation of γ to neutron branching ratios is presented in Sec. VI and compared with Hauser-Feshbach calculations in Sec. VII, together with a discussion of the possible impact on neutron-capture cross-section estimates for unstable very neutron-rich nuclei. Partial results of the work presented here were already published in Ref. [9].

A. Reactor decay heat

A knowledge of the heating produced by radioactive products in a reactor and its time evolution after reactor shutdown is important for reactor safety. In conventional reactors the DH is dominated by FP for cooling times up to a few years. An issue in reactor DH studies has been the persistent failure of summation calculations to reproduce the results of integral experiments for individual fissioning systems. Summation calculations are based on individual FP yields and average γ-ray and β energies retrieved from evaluated nuclear databases. In spite of this deficiency, summation calculations remain an important tool in reactor safety studies. For example, after the Fukushima Dai-ichi nuclear plant accident, it was pointed out [10] that summation calculations are relevant to understand the progression of core meltdown in this type of event. The Fukushima accident was the consequence of a failure to dissipate effectively the DH in the reactor core and in the adjacent spent-fuel cooling pool. Summation calculations are particularly important in design studies of innovative reactor systems (Gen IV reactors, accelerator-driven systems) with unusual fuel compositions (large fraction of minor actinides), high burn-ups, and/or harder neutron spectra, since integral data are missing.

Yoshida and Nakasima [11] recognized that the Pandemonium systematic error is responsible for a substantial fraction of the discrepancy between DH integral experiments and calculations. The average γ and β energy for each isotope, $\bar{E}_\gamma$ and $\bar{E}_\beta$ respectively, can be computed from $I_\beta(E_x)$, the β-intensity distribution as a function of excitation energy E_x, as

$$\bar{E}_\gamma = \int_0^{Q_\beta} I_\beta(E_x) E_x dE_x, \tag{1}$$

$$\bar{E}_\beta = \int_0^{Q_\beta} I_\beta(E_x) \langle E_\beta(Q_\beta - E_x)\rangle dE_x. \tag{2}$$

Here $\langle E_\beta(Q_\beta - E_x)\rangle$ represents the mean value of the β-energy continuum leading to a state at E_x. According to Eqs. (1) and (2), the pandemomium systematic error affecting HRGS data has the effect of artificially decreasing the average γ-ray energy and increasing the average β energy.

The TAGS technique, free from Pandemonium, was applied in the 1990s by Greenwood and collaborators at INEL (Idaho) [12] to obtain accurate average decay energies for up to 48 FP with impact in DH calculations. Recognizing the importance of this approach to improving summation calculations, the OECD/NEA Working Party on International Evaluation Cooperation (WPEC) established subgroup SG25 to review the situation [13]. Recommendations were made, in the form of priority lists, for future TAGS measurements on specific isotopes for the U/Pu fuel cycle. The work was later extended to the Th/U fuel cycle by Nichols and collaborators [14]. The results of Algora *et al.* [15] demonstrated the large impact of new TAGS measurements for a few isotopes selected from the priority list.

From the nuclei included in the present work ^{87}Br was assigned priority 1 in Refs. [13,14] for a TAGS measurement, although it is an example of a well-studied level scheme [1] with up to 374 γ transitions de-exciting 181 levels. The justification for the high priority comes from (1) the large

uncertainty (25%) on average energies coming from the spread of intensity normalization values between different measurements, (2) a potential Pandemonium error suggested by the number of observed levels at high excitation energies (less than half of the expected number according to level density estimates), and (3) the large contribution to DH around 100 s cooling time. ^{88}Br also has priority 1 in Refs. [13,14]. It contributes significantly to the DH at cooling times around 10 s. The known decay scheme [2] is rather incomplete above $E_x = 3.5$ MeV, from level density considerations, as shown in the RIPL-3 reference input parameter library web page [17]. We estimate that more than 300 levels should be populated in the decay above $E_x = 3.5$ MeV and below S_n in comparison with the observed number of 33. ^{94}Rb is not included in the priority list of Ref. [13] but is considered to be of relative importance in Refs. [14] and [16] for short cooling times. The decay scheme is very poorly known [3]. Only 37 levels are identified above $E_x = 3.4$ MeV, regarded as the maximum energy with a complete level scheme [17]. We estimate that more than 900 levels could be populated below S_n, thus pointing to a potentially strong Pandemonium effect.

B. Reactor antineutrino spectrum

An accurate knowledge of the reactor antineutrino $\bar{\nu}_e$ spectrum is of relevance for the analysis of neutrino oscillation experiments [18,19] and for exploring the use of compact antineutrino detectors in nuclear proliferation control [20]. Summation calculations are also a valuable tool to obtain the $\bar{\nu}_e$ spectrum but suffer from the same problem as DH summation calculations: inaccuracies in fission yields and individual precursor decay data.

For each fission product the electron antineutrino spectrum $S_{\bar{\nu}}(E_{\bar{\nu}})$, and the related β spectrum $S_\beta(E_\beta)$, can be computed from the β-intensity distribution

$$S_{\bar{\nu}}(E_{\bar{\nu}}) = \int_0^{Q_\beta} I_\beta(E_x) s_{\bar{\nu}}(Q_\beta - E_x, E_{\bar{\nu}}) dE_x, \quad (3)$$

$$S_\beta(E_\beta) = \int_0^{Q_\beta} I_\beta(E_x) s_\beta(Q_\beta - E_x, E_\beta) dE_x, \quad (4)$$

where $s_{\bar{\nu}}(Q_\beta - E_x, E_{\bar{\nu}})$ and $s_\beta(Q_\beta - E_x, E_\beta)$ represent the shape of $\bar{\nu}_e$ and β energy distributions for the transition to a state at E_x. For each E_x, $s_{\bar{\nu}}$ and s_β are related by energy conservation $E_{\bar{\nu}} = Q_\beta - E_x - E_\beta$ to a good approximation. Thus distortions of the observed $I_\beta(E_x)$ distribution in HRGS due to Pandemonium tend to produce calculated $\bar{\nu}_e$ spectra shifted to higher energies.

Currently the most reliable reactor $\bar{\nu}_e$ spectra are obtained from integral β-spectrum measurements of ^{235}U, ^{239}Pu, and ^{241}Pu thermal fission performed by Schreckenbach *et al.* at ILL-Grenoble [21,22]. Data on ^{238}U fast fission also became available recently [23]. The conversion of integral β spectra to $\bar{\nu}_e$ spectra requires a number of approximations. These are needed because, as pointed out above, the transformation is isotope and level dependent. The global conversion procedure has been revised and improved recently [24,25]. As a consequence of this revision, a change of normalization in the detected spectrum is found that contributes to a consistent deficit when comparing $\bar{\nu}_e$ rates from short baseline experiments with calculations [26], a surprising effect which is termed the *reactor neutrino anomaly*. The possibility that the deficit is related to the existence of sterile neutrinos has aroused considerable interest. On the other hand, several sources of systematic error could explain the anomaly. In particular, the effect could be related to an abundance of transitions of the first forbidden type [27] for which the spectral shape is not well known. The β spectrum depends in this case on the nuclear wave functions, departing from the allowed shape. In addition, higher order corrections to the shape, mainly the weak magnetism correction dependent on transition type, play a significant role. Nuclear structure calculations [28] also show the relevance of using the correct β shape for individual decay branches. The experimental investigation of this or similar effects benefits from accurate decay measurements of individual fission products and the use of the summation method, as was argued in Ref. [29].

The statistics accumulated in the three running reactor $\bar{\nu}_e$ experiments, Double Chooz [30], RENO [31], and Daya Bay [32], has revealed differences between the shape of the calculated $\bar{\nu}_e$ spectra and the measured one. Several possible sources for the shape distortion have been discussed [33]. The observed excess between 5 and 7 MeV $E_{\bar{\nu}_e}$ could be due to the contribution of a few specific FP [34,35], which is not reproduced by the global conversion method. Thus the study of this new antineutrino shape distortion requires the use of the summation method and reinforces the need for new accurate decay data with the TAGS technique. As a matter of fact, one of the key isotopes in this list, ^{92}Rb, was part of the same experiment analyzed here and its impact on the antineutrino spectrum was already evaluated [36]. From the isotopes studied in the present work ^{94}Rb has an appreciable contribution to the high-energy part of the $\bar{\nu}_e$ spectrum.

Another approach to the improvement of decay data for both $\bar{\nu}_e$ and DH summation calculations was followed in the past by Tengblad *et al.* [37]. They measured the spectrum of electrons emitted in the decay of individual FP using charged particle telescopes. This method is in essence Pandemonium free. Measurements were performed for up to 111 fission products at ISOLDE (Geneva) and OSIRIS (Studsvik). The β spectra are converted into $\bar{\nu}_e$ spectra and both are tabulated for 95 isotopes in Ref. [38]. It was first pointed out by Bersillon during the work of WPEC-SG25 [13] that average β energies from Tengblad *et al.* [37] can be compared with average β energies calculated from TAGS data obtained by Greenwood *et al.* [12] (see also Subsec. I A) for up to 18 fission products. The comparison shows that $\bar{E}_\beta$ energies from Tengblad *et al.* are systematically larger than those from Greenwood *et al.* The average difference is +177 keV with a spread of values from −33 to +640 keV. In view of the relevance of both sets of data it is important to confirm the discrepancy and investigate possible causes. The list of measured isotopes in [37,38] includes ^{87,88}Br and ^{94}Rb; thus, they can be compared with our data.

C. γ-ray emission from neutron unbound states

Neutron-unbound states can be populated in the β decay of very neutron-rich nuclei, when the neutron separation

energy S_n in the daughter nucleus is lower than the decay energy window Q_β. The relative strength of strong and electromagnetic interactions determines that typically neutron emission from these states predominates over γ-ray emission. These emission rates are quantified by the partial level widths Γ_n and Γ_γ respectively. The fraction of β intensity followed by γ-ray emission is given by $\Gamma_\gamma/\Gamma_{\rm tot}$, with $\Gamma_{\rm tot} = \Gamma_\gamma + \Gamma_n$. There is an analogy [39] between this decay process and neutron capture reactions populating unbound states. Such resonances in the compound nucleus re-emit a neutron (elastic channel) or de-excite by γ rays (radiative capture). Indeed, the reaction cross section is parametrized in terms of neutron and γ widths. In particular the (n,γ) cross section includes terms proportional to $\Gamma_\gamma\Gamma_n/\Gamma_{\rm tot}$. Notice that the spins and parities of states populated in β decay and (n,γ) do not coincide in general because of the different spin and parity of the respective parent and target nuclei and the different selection rules.

Neutron capture and transmission reactions have been extensively used [40] to determine Γ_γ and Γ_n of resolved resonances, or the related strength functions in the unresolved resonance region. An inspection of Ref. [40] shows that in general Γ_n is measured in eV or keV while Γ_γ is measured in meV or eV, in agreement with expectation. Current data are restricted, however, to nuclei close to stability since such experiments require the use of stable or long-lived targets. On the other hand, (n,γ) capture cross sections for very neutron-rich nuclei are a key ingredient in reaction network calculations describing the synthesis of elements heavier than iron during the rapid (r) neutron-capture process occurring in explosive-like stellar events. In the classical picture of the r-process [41] a large burst of neutrons synthesizes the elements along a path determined by the $(n,\gamma)-(\gamma,n)$ equilibrium. After the exhaustion of neutrons these isotopes decay back to the valley of β stability. In this simplified model the capture cross section magnitude plays no role. However, it is known [42–44] that for realistic irradiation scenarios the final elemental abundance is sensitive to the actual (n,γ) cross sections. This is the case for the hot (classical) r process, due to the role of late captures during the decay back to stability. It is also the case for a cold r-process, where the formation path is determined by competition between neutron capture and β decay.

Lacking experimental information, the cross section for these exotic nuclei is typically obtained from Hauser-Feshbach statistical model calculations [45]. This model is based on a few quantities describing average properties of the nucleus: the nuclear level density (NLD), the photon strength function (PSF), and the neutron transmission coefficient (NTC). The PSF determines Γ_γ, NTC determines Γ_n, and NLD affects both (see the appendix). The parameters describing the dependence of these quantities on various magnitudes are adjusted to experiment close to β stability. It is thus crucial to find means to verify the predictions of the model far from stability. For example, the use of surrogate reactions with radioactive beams and inverse kinematics has been suggested as a tool to provide experimental constraints on (n,γ) cross sections [46] for unstable nuclei, but its application is very challenging and, considering limitations on beam intensities, probably limited to nuclei not far from stability at present. On the other hand, the study of γ-ray emission from states above S_n observed in β decay can give quantitative information on $\Gamma_\gamma/\Gamma_{\rm tot}$ for unstable nuclei. This information can be used to improve neutron capture cross-section estimates for nuclei far away from β stability.

The emission of γ rays from neutron unbound states populated in β decay has been observed in very few cases studied with high-resolution germanium detectors. It was first detected in 1972 in the decay of ^{87}Br [47], which remains one of the best studied cases [48–50]. The other cases are ^{137}I [51–53], ^{93}Rb [12,54,55], ^{85}As [52,56], ^{141}Cs [57], ^{95}Rb [58], ^{94}Rb [55], ^{77}Cu [59], and ^{75}Cu [60]. In the decay of ^{87}Br up to a dozen states emitting single γ rays have been identified within 250 keV above S_n, with a total intensity of about 0.5% compared with a neutron emission intensity of 2.6%. The observation of relatively intense γ rays in this measurement was explained as being due to nuclear structure since some of the levels populated could only decay through the hindered emission of a high orbital angular momentum neutron. On the other hand, it was pointed out [61] that a sizable γ-ray emission from neutron unbound states could be a manifestation of Porter-Thomas (PT) statistical fluctuations in the strength of individual transitions. The extremely asymmetric shape of the PT distribution can lead to very large enhancement of the $\Gamma_\gamma/\Gamma_{\rm tot}$ ratio with respect to the average. However, a general characterization of the phenomenon is still lacking, in particular the relative importance of the different mechanisms governing the competition.

It is difficult to pursue these studies using HRGS because of its reduced sensitivity. TAGS can offer the required sensitivity at high excitation energy. However, its application is challenging, since the expected γ branching is very small. As a matter of fact, previous attempts at the Leningrad Nuclear Physics Institute (LNPI) [55] did not lead to clear conclusions. As we have shown in Ref. [9], and further discuss here, the TAGS technique can extract accurate information on the γ emission above S_n provided the possible sources of systematic error are under control.

The isotopes selected for this study are β-delayed neutron emitters with well-known decay parameters (see Table I) that are located either close to the β-stability valley (^{87,88}Br) or relatively far away (^{94}Rb). In particular, ^{87}Br was included since it allows a comparison of our results with neutron capture and transmission experiments [50,62] and with high-resolution decay measurements [50]. An additional reason for their inclusion is that the spectrum of β-delayed neutrons is known [63,64] for all of them and the neutron branching to the levels in the final nucleus has been studied [1–3]. This allows the reconstruction of the β-intensity distribution followed by neutron emission and a more detailed comparison of γ to neutron branching ratios with calculations (see Sec. VII).

The case of ^{93}Rb was also measured [65] but will be presented separately.

II. MEASUREMENTS

The measurements were performed at the Cyclotron Laboratory of the University of Jyväskylä. The isotopes of interest are produced by proton-induced fission of uranium in the ion-guide source of the IGISOL Mass Separator [66]. The

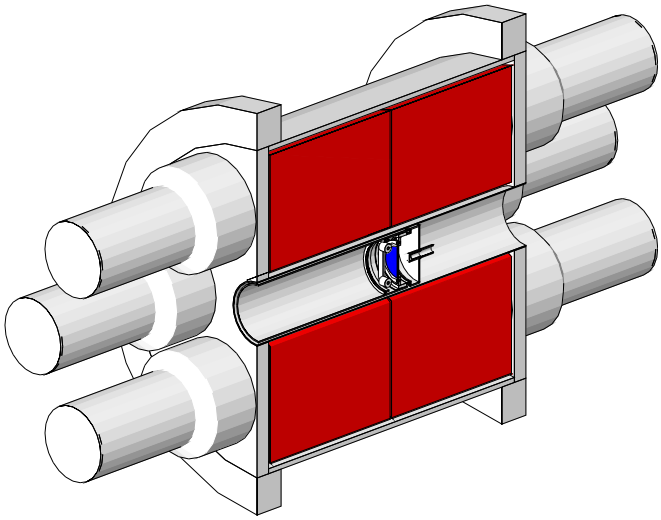

FIG. 1. Cross-sectional view of the detector geometry as implemented in the GEANT4 simulation code. BaF_2 crystals in red. Si detector in blue. The beam enters from the left and is deposited on the tape (not shown in the figure) in front of the Si detector.

mass separated beam is guided to the JYFLTRAP Penning Trap [67], for suppression of contamination. The JYFLTRAP mass resolving power of few tens of thousands is sufficient to select the isotope of interest from the rest of isobars. The beam coming out of the trap is implanted at the center of the spectrometer onto a movable tape, in between two rollers holding the tape in place. A cross-sectional view of the detection setup is shown in Fig. 1 and a detailed view of the beam-tube end cap is shown in Fig. 2. The tape is an ordinary half-inch computer tape made of Mylar with a thickness of 30 μm and a 10-μm magnetic layer facing the beam. During the measurements the beam gate is open for a time period equivalent to three half-lives. This optimizes the counting of parent decays over descendant decays. After this period of time, the tape transports the remaining activity away and a new measuring cycle starts. The tape moves inside an evacuated aluminium tube of 1 mm thickness and 47 mm diameter. Behind the tape implantation point is placed a 0.5-mm-thick Si detector with a diameter of 25 mm, mounted on the aluminium

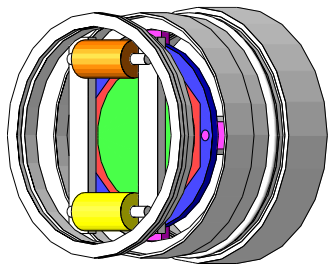

FIG. 2. View of the beam-tube end-cap geometry as implemented in the GEANT4 simulation code. Visible elements are the detector holder (blue), holder screws and mounts (pink), silicon detector (red) with active area (green), aluminium roller (yellow), plastic roller (orange), and aluminium structural elements (white). For clarity the tape is not shown.

end cap. The β-detection efficiency of the Si detector is about 30%. The Valencia-Surrey Total Absorption Spectrometer "Rocinante" is a cylindrical 12-fold segmented BaF_2 detector with a length and external diameter of 25 cm, and a longitudinal hole of 5 cm diameter. Each BaF_2 crystal is optically isolated by means of a thin reflector wrapping, and viewed by a single 3-in. photomultiplier tube (PMT). The crystals are mounted inside the aluminium housing, which has a 0.8-mm-thick wall around the central hole. The total efficiency of Rocinante for detecting a single γ ray with the setup described here is larger than 80% in the energy range of interest. The spectrometer is surrounded by 5-cm-thick lead shielding to reduce the detection of the ambient background signals.

The new spectrometer has a reduced neutron sensitivity compared to existing instruments based on NaI(Tl) crystals. This is a key feature in the present measurements, as will be shown later. In addition, the segmentation of the detector allows one to obtain information on γ-ray cascade multiplicities which helps in the data analysis. The signal amplitudes from the 12 independent PMTs are digitized in a peak sensing analog-to-digital converter (ADC) and stored on disk for each event. The event trigger is provided whenever the hardware sum of the PMT signals fires a constant fraction discriminator (CFD). The signal from the Si detector is processed in an analogous manner, providing another trigger for readout and storage of events. In the off-line analysis the PMT signals are gain matched and those surpassing a common threshold of 65 keV are added to obtain the total absorption spectrum. The gain-matching procedure uses as a reference the position of the α peaks visible in the energy spectra coming from the Ra contamination always present in BaF_2 crystals. In order to eliminate this intrinsic background as well as the ambient background we use in the present analysis β-gated total absorption spectra. The threshold in the Si β detector is set to 100 keV. Nevertheless, other sources of background need to be taken into account.

First, there is the decay descendant contamination, which was computed using Monte Carlo (MC) simulations performed with the GEANT4 simulation toolkit [68]. In the case of daughter decay contamination (^{87}Kr, ^{88}Kr, ^{94}Sr) we use an event generator based on β-intensity distributions and γ branching ratios obtained from the decay scheme in Refs. [1–3], which we assume is sufficiently well known. The normalization of the daughter contamination is estimated from the known half-lives and the measurement cycle time information and eventually adjusted to provide the best fit to the recorded spectrum. The measurement of ^{88}Br was accidentally contaminated with ^{94}Y, the long-lived grand-daughter of ^{94}Rb that was measured immediately beforehand. It was treated in the same manner.

The contamination due to the β-delayed neutron branch is more challenging. The decay simulation must explicitly include the neutrons emitted. These neutrons interact with detector materials, producing γ rays through inelastic and capture processes, which are readily detected in the spectrometer. The event generator should reproduce the known neutron energy distribution, taken from Ref. [64]; the known γ-ray intensity in the final nucleus, taken from Refs. [1–3]; and the correct decay sequence $\beta \rightarrow$ neutron $\rightarrow \gamma$. Thus the event generator needs the β-intensity distribution followed by

neutron emission $I_{\beta n}(E_x)$. This can be obtained by deconvolution of the measured neutron energy spectrum $S(E_n)$, taking into account the relation

$$S(E_n) = \int_{S_n}^{Q_\beta} \left\langle \frac{\Gamma_n(E_x, E_n)}{\Gamma_n(E_x)} \right\rangle I_{\beta n}(E_x) dE_x, \quad (5)$$

where $\langle \Gamma_n(E_x, E_n)/\Gamma_n(E_x) \rangle$ represents the neutron branching to levels in the final nucleus with excitation energy $E_x^f = E_x - S_n - E_n$ (see the appendix). The neutron branching ratio can be calculated using the Hauser-Feshbach model and this is done to obtain the $I_{\beta n}(E_x)$ distribution used later in the present work. However, the calculated $\langle \Gamma_n(E_x, E_n)/\Gamma_n(E_x) \rangle$ do not reproduce the observed γ-ray intensities in the final nucleus. Thus, for the purpose of simulating the contamination due to β-delayed neutron decays, we follow a different approach. We use the simplifying assumption that the neutron branching to each excited level in the final nucleus is independent of the excitation energy in the daughter nucleus. Then we can define partial decay intensities proportional to the neutron spectrum with energies larger than the excitation energy of the level f in the final nucleus, $I_{\beta n}^f(E_x) = I_n^f S(E_x - S_n - E_x^f)$. The proportionality constant I_n^f is just the measured neutron branching. The partial intensity to the ground state is obtained as the difference between the total neutron spectrum and the partial spectra. We found that the $I_{\beta n}(E_x)$ distribution obtained in this manner is not very different from the one obtained by deconvolution.

A different issue related to the reproduction of the contamination coming from the β-delayed neutron branch is whether the interaction of neutrons with the detector can be simulated accurately. We have shown recently [69] this to be the case for a $LaBr_3$:Ce detector, provided that GEANT4 is updated with the newest neutron data libraries and the original capture cascade generator is substituted by an improved one based on the nuclear statistical model. We have followed the same approach for our BaF_2 detector. The normalization factor of the β-delayed neutron decay contamination is fixed by the P_n value.

An important source of spectrum distortion is the summing pileup of events. If more than one event arrives within the same ADC event gate, a signal with the wrong energy will be stored in the spectrum. Apart from the electronic pulse pileup effect for a single crystal, which can be calculated using the methodology described in Ref. [70], one must consider the summing of signals from different crystals. A new Monte Carlo procedure to calculate their combined contribution has been developed. The procedure is based on the superposition of two recorded events, selected randomly. The time of arrival of the second event is sampled randomly within the ADC gate length. The normalization of the resulting summing-pileup spectrum is fixed by the true rate and the ADC gate length [70]. To calculate the rate, a dead time correction is necessary, and this is obtained by counting the signals from a fixed frequency pulse generator feeding the preamplifier. The use of real events to calculate the spectrum distortion is valid if the actual summing-pileup rate is small enough. For this reason we kept the overall rate during the measurements below 7 kcps. The method is validated with measurements of laboratory sources.

Several sources, ^{22}Na, ^{24}Na, ^{60}Co, and ^{137}Cs, were used to determine both the energy calibration and the resolution versus energy dependency of the spectrometer. The latter is needed to widen the MC simulated response and is parametrized in the form of a Gaussian with $\sigma_E = \sqrt{aE + bE^2}$. The highest calibration point is at 4.123 MeV. At this energy, the energy resolution (FWHM) is 265 keV, which becomes 455 keV at 10 MeV. The ungated spectra measured with the sources serve also to verify the accuracy of the GEANT4 MC simulations of the spectrometer response to the decay. This requires a detailed description in the simulation code of all materials in the measurement setup including detectors and the tape transport system. Figures 1 and 2 show details of the geometry implemented in GEANT4.

The use of β-gated spectra in the analysis requires additional verifications of the simulation. Due to the existence of an electronic threshold in the Si detector (100 keV) and the continuum nature of the β spectrum, the efficiency for β detection has a strong dependency with endpoint energy up to about 2 MeV. It should be noted that this affects the spectral region above S_n in which we are particularly interested. To investigate whether the MC simulation can reproduce this energy dependency accurately, we used the information from a separate experiment [71] measuring P_n values with the neutron counter BELEN and the same β detector and implantation setup. Several β-delayed neutron emitters with known neutron energy spectra were measured, including ^{88}Br, ^{94,95}Rb, and ^{137}I. They have different neutron emission windows $Q_\beta - S_n$; therefore, the neutron-gated β efficiency samples different portions of the low-energy part of the efficiency curve. Indeed, the measured average β detection efficiency for each isotope changes by as much as 25%. Using the above-mentioned β-delayed neutron decay generator in GEANT4 we are able to reproduce the isotope-dependent efficiency to within better than 4%, determining the level of accuracy of the simulation.

Figure 3 shows the β-gated TAGS spectrum measured for all three isotopes. Also shown is the contribution to the measured spectra of the daughter decay, the neutron decay branch, and the summing-pileup effect. In the case of ^{88}Br it also includes the contribution of the accidental contamination with ^{94}Y decay. Note that there are net counts above the background beyond the neutron separation energy. The fraction of counts that are to be attributed to states above S_n populated in the decay de-exciting by γ-ray emission is obtained after deconvolution with the spectrometer response. In this region, the major background contribution comes from summing pileup, which is well reproduced by the calculation, as can be observed. The contribution of neutron-capture γ rays in the detector materials is much smaller, thanks to the low neutron sensitivity of BaF_2, as can be seen. The contribution of γ rays coming from neutron inelastic scattering is important at energies below 1 MeV.

III. ANALYSIS

The analysis of the β-gated spectra follows the method developed by the Valencia group [72,73]. The deconvolution of spectra with the spectrometer response to the decay is performed using the expectation-maximization (EM) algorithm described there. The spectrometer response is constructed in two steps. First, the response to electromagnetic cascades is calculated from a set of branching ratios and the MC

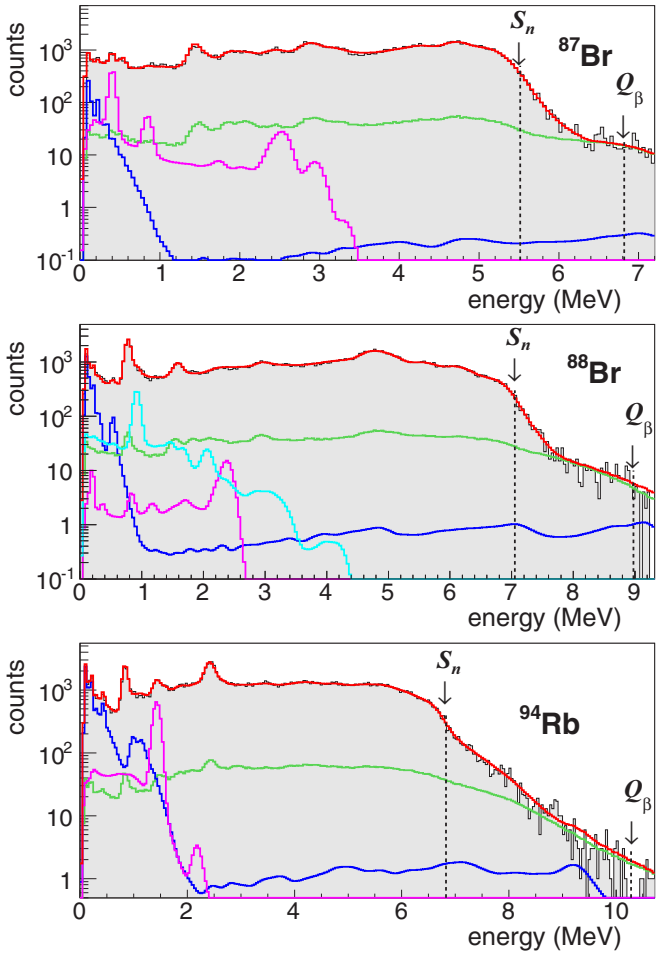

FIG. 3. Relevant histograms for the analysis: parent decay (gray filled), daughter decay (pink), delayed neutron decay (dark blue), accidental contamination (light blue), summing-pileup contribution (green), and reconstructed spectrum (red). See text for details. The neutron separation energy S_n and decay energy window Q_β are also indicated.

calculated response to individual γ rays. In the simulation, we use a single-crystal low-energy threshold of 65 keV from the experiment. When necessary, the electron conversion process is taken into account while building the response [74]. Branching ratios are taken from [1–3] for the low-energy part of the level scheme. In the present case, this involves 4 levels up to 1.6 MeV for ^{87}Kr, 8 levels up to 2.5 MeV for ^{88}Kr, and 11 levels up to 2.8 MeV for ^{94}Sr. The excitation energy range above the last discrete level is treated as a continuum and is divided into 40-keV bins. Average branching ratios for each bin are calculated from the NLD and PSF as prescribed by the nuclear statistical model (see the appendix). We use the NLD calculated using a Hartree-Fock-Bogoliubov (HFB) plus combinatorial approach adjusted to experimental information [17,75], which includes parity dependence. The PSF is obtained from generalized Lorentzian ($E1$ transitions) or Lorentzian ($M1$ and $E2$ transitions) parametrization using the parameters recommended in the RIPL-3 reference input parameter library [17]. In the second step of the response construction, the previously obtained electromagnetic response for each level or energy bin is convoluted with the simulated response to a β continuum of allowed shape. The β response is obtained under the condition that the energy deposited in the Si detector is above the 100-keV threshold.

The spins and parities of some of the discrete states in the daughter nucleus are ambiguous but they are needed in order to calculate the branching ratio from states in the continuum. In the analysis, different spin-parity values are tested and those giving the best fit to the spectrum are taken. The spin and parity of the parent nucleus ground state are also uncertain; however, they determine the spin and parity of the states populated in the continuum needed to construct the branching ratio matrix. We assume that the Gamow-Teller selection rule applies for decays into the continuum, i.e., the parity does not change and the spin change fulfills $|\Delta J| \leqslant 1$. In the calculation of the branching ratios we further assume that different spins J are populated according to the spin statistical weight $2J + 1$. Our choices of spin and parity for the ground state are $3/2^-$ for ^{87}Br, 1^- for ^{88}Br, and 3^- for ^{94}Rb, based again on the quality of reproduction of the measured spectra. The spin parity of ^{87}Br is given as $3/2^-$ in Ref. [1]; however Ref. [76] proposes $5/2^-$. We do not find significant differences in the analysis assuming these two values and we choose the former. The spin parity of ^{88}Br is uncertain and is given as (2^-) in Ref. [2]. However, Ref. [77] suggests 1^-. In our analysis we use the latter value since it clearly provides a much better reproduction of the measured TAGS spectrum. In the case of ^{94}Rb , $3(^-)$ is proposed [3] and is adopted, since other alternatives did not lead to a better reproduction of the spectrum.

In the analysis, we permit decays to all discrete states, many of which are of the forbidden type. Forbidden transitions to the ground state or low-lying excited states are known to occur in this region of the nuclear chart. Indeed, sizable decay intensity for some forbidden transitions is obtained in our analysis. In the case of ^{87}Br, we find a ground-state intensity $I_\beta^{gs} = 10.1\%$ quite close to 12%, the quoted value in Ref. [1]. However, in contrast to Ref. [1], the first four excited states included in the discrete part receive negligible intensity. The summed decay intensity to the discrete part becomes 51% of that in Ref. [1]. In Ref. [2] an upper limit of 11% is given for the ^{88}Br ground-state decay intensity, and a sizable intensity is quoted for some of the eight excited states included in the analysis. We obtain 4.7% and 5.6% for the β intensity to the ground state and first excited state respectively, and small or negligible intensity for the remaining states. Overall, the intensity to this part of the level scheme is reduced by 64%. No intensity is assigned in Ref. [3] to ^{94}Rb decaying to the ground state (third forbidden) and first excited state (first forbidden). In our analysis, we forbid the decay to those states after verifying that the decay intensity obtained when left free is only 0.5% and 0.02% respectively. A large decay intensity of 23.7% is observed for the allowed transition to the state at $E_x = 2414$ keV, even larger than the value of 21.4% found in Ref. [3]. The intensity to the discrete level scheme included in our analysis (11 states) is 78% of that in ENSDF.

In the final analysis, we applied a correction to branching ratios deduced from the statistical model. The aim is to obtain a spectrometer response that is as realistic as possible.

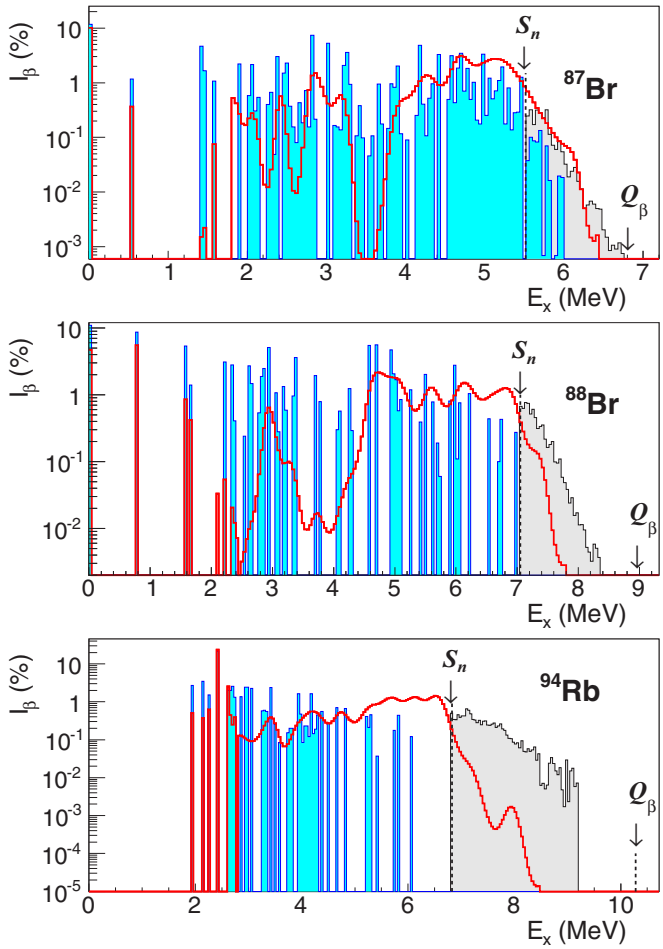

FIG. 4. β-intensity distributions: TAGS result (red line), high-resolution measurements (blue filled), from delayed neutron spectrum (gray filled). See text for details.

We scale the calculated branching ratios, going from the unknown part of the level scheme to discrete levels in the known part of the level scheme, in order to reproduce the observed γ-ray intensities as tabulated in Refs. [1–3]. Here we are making the assumption that the absolute γ intensity is correctly determined in HRGS measurements for the lowest excited levels. We found that this adjustment did not lead to significant changes in the quality of reproduction of the measured TAGS spectra and has a small impact on the results of the deconvolution.

Figure 4 shows the final β-intensity distribution $I_{\beta\gamma}(E_x)$ resulting from the deconvolution of TAGS spectra for all three isotopes with the chosen branching ratio matrices. The intensity is normalized to $(100 - P_n)\%$. In each case, the spectrum reconstructed with this intensity distribution gives a good reproduction of the measured spectrum, as can be seen in Fig. 3. The full β-intensity distribution including statistical uncertainties is given as the Supplemental Material to this article [78]. The uncertainty due to the statistics in the data is computed according the prescription given in Ref. [73] and is very small.

We evaluate the impact of several sources of systematic uncertainty on the shape of the β-intensity distribution. These include both uncertainties in the calculated decay response and uncertainties in the subtraction of background components. To study their effect, we follow a similar procedure in all the cases. The chosen systematic parameter is varied and a new deconvolution is performed until we observe an appreciable deterioration in the reproduction of the measured spectrum. This is quantified by the increase of χ^2 between the measured and reconstructed spectra. In this way, we obtain the maximum acceptable deviation of the $I_{\beta\gamma}(E_x)$ from the adopted solution for each investigated systematic uncertainty. As a reference, the maximum χ^2 increase found is always below 5%.

Uncertainties in the calculated decay response are of two types: uncertainties in the branching ratio matrix, which were discussed above, and uncertainties in the MC simulation of the response to γ and β radiation. As already explained, we take great care to describe accurately the geometry used in the GEANT4 simulation, which is validated from the comparison with measurements with laboratory sources. However, these sources emit β particles with rather low energies and they are not useful to verify the β response. The simulated β efficiency of the Si detector and in particular its variation with endpoint energy was studied in a separate measurement [71], as already discussed. The response of the spectrometer to β particles depositing energy in the Si is not easy to verify. The response is a mixture of β penetration and secondary radiation produced in dead materials. The accurate simulation of the interaction of low energy electrons is a challenging task for any MC code. They rely on models to describe the slowdown of electrons and changes in their trajectory. Typically, a number of tracking parameters are tuned to obtain reliable results. We use in the present simulations the Livermore Electromagnetic Physics List of GEANT4 (version 9.2.p2) with original tracking parameters. This physics list has been developed for high accuracy tracking of low energy particles. We verified that limiting the tracking step length (parameter StepMax) to values much smaller than default values increased computing time considerably but did not significantly affect the simulated response. Still, the true response can differ from the simulation both in shape and magnitude and the differences can be endpoint energy dependent. To study the effect of a possible systematic error on the β response, we take a crude approach, ignoring changes in shape and any dependence on endpoint energy. We scale arbitrarily the simulated spectrometer response while keeping the same β efficiency. In this way we find that solutions corresponding to changes of $\pm 10\%$ in the β response normalization represent the maximum deviation with respect to the adopted solution that can be accepted.

The individual γ response is well tested up to $E_\gamma = 2.754$ MeV, the maximum energy for the ^{24}Na source. To investigate the effect of a possible systematic error in the total γ efficiency ε_γ or in the peak-to-total ratio (P/T) we introduce a model that varies linearly with energy one of the two parameters, ε_γ or P/T, above $E_\gamma = 3$ MeV. We found that variations of ε_γ amounting to $\pm 15\%$ at $E_\gamma = 10$ MeV or variations of P/T amounting to $\pm 30\%$ at the same energy are the maximum allowed by good reproduction of the spectrum. When considering these numbers, one should bear in mind that the de-excitation of highly excited states populated in the decay of the three isotopes proceeds with an average γ multiplicity

of 2 to 4 in such a way that the energy of most γ rays in the decay does not exceed 3 MeV.

Uncertainties in the normalization of background components also have an impact on the β-intensity distribution. We consider the two main components, summing pileup, which affects the high-energy part of the spectrum, and the β-delayed neutron decay branch, which affects the low-energy part of the spectrum (see Fig. 3). The component due to summing pileup is normalized using the same ADC gate length (5 μs) for all three isotopes. We estimate, however, that the reproduction of the end part of the spectra allows for a variation of up to $\pm 15\%$ in the normalization factor. The normalization of the β-delayed neutron-decay component is fixed by the P_n value. Likewise, we find that the reproduction of the low-energy part of the spectrum allows for a variation of up to $\pm 15\%$ in the normalization factor.

Finally, we also check the impact on the result associated with the use of a different deconvolution algorithm, by using the maximum entropy method as described in Ref. [73]. This leads to changes in the $I_\beta(E_x)$ noticeable both at the high-energy end and at low E_x.

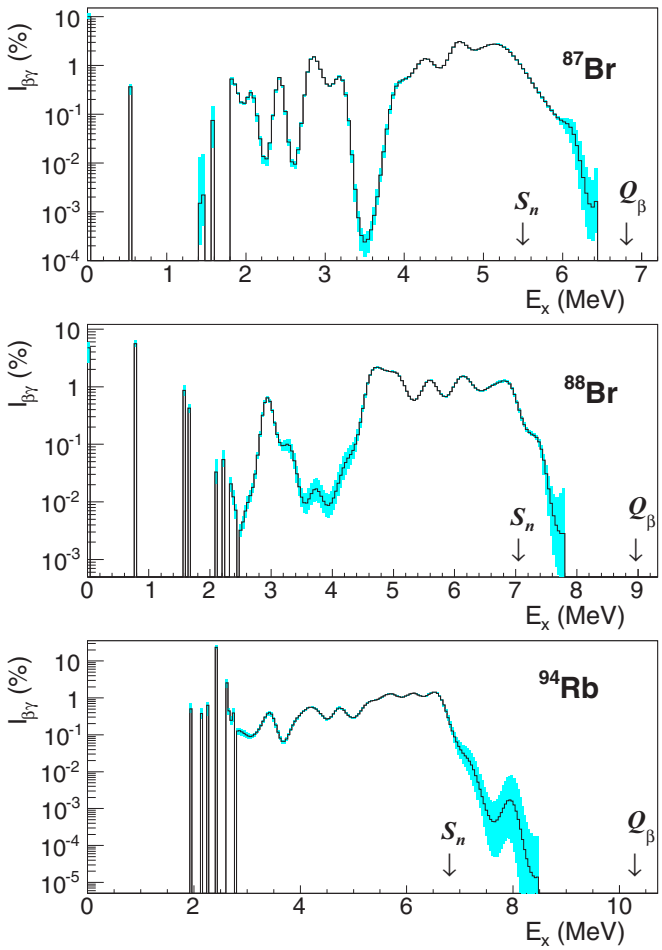

FIG. 5. β-intensity distributions from TAGS. The thin black line is the adopted solution; the light-blue filled region indicates the spread of solutions due to the systematic effects investigated. See text for details.

There is no straightforward way to quantify and combine the systematic uncertainties associated with the effects investigated. One of the reasons is that they are not independent since we are requiring reproduction of the data. It would have been a formidable task to explore in a correlated way the full parameter space. We use a different point of view here. The solutions we obtain through the systematic variation of each parameter represent maximum deviations from the adopted solution and thus altogether define an estimate of the space of solutions compatible with the data. This is represented in a graphical way in Fig. 5, showing the envelope of the different solutions described above corresponding to the maximum accepted deviation from the adopted solution. In total there are 14 solutions for ^{87}Br, 13 for ^{88}Br, and 15 for ^{94}Rb. As can be seen, the different solutions differ little except for specific E_x regions, where the β intensity is low, in particular at the high-energy end of the distribution.

IV. AVERAGE β- AND γ-DECAY ENERGIES AND DECAY HEAT

Figure 4 shows in addition to $I_{\beta\gamma}(E_x)$ obtained from our TAGS data the intensity obtained from HRGS measurements retrieved from the ENSDF database [1–3]. The effect of Pandemonium is visible here. Our results show a redistribution of $I_{\beta\gamma}(E_x)$ towards high E_x, which is significant for ^{87}Br and very large for ^{88}Br and ^{94}Rb. This is even clearer in the accumulated β-intensity distribution as a function of excitation energy $I^{\Sigma}_{\beta\gamma}(E_x) = \int_0^{E_x} I_{\beta\gamma}(E)dE$, depicted in Fig. 6. The intensity is normalized to $100\% - P_n$ except in the case of the ^{94}Rb ENSDF intensity that only reaches 59.8% since the evaluators of Ref. [3] recognize the incompleteness of the decay scheme.

Table II shows $\bar{E}_\gamma$ and $\bar{E}_\beta$ obtained from $I_{\beta\gamma}(E_x)$ using Eqs. (1) and (2), respectively. The β continuum and its average energy $\langle E_\beta(Q_\beta - E_x)\rangle$ for each E_x is calculated using subroutines extracted from the LOGFT program package maintained by NNDC (Brookhaven) [79]. In the calculations, we assume an allowed β shape. As can be seen in Table II, the redistribution of β intensity leads to large differences in the average emission energies when comparing HRGS data (ENSDF) and the present TAGS data. The difference has opposite directions for γ and β energies, as expected, except in the case of ^{94}Rb due to the use of a different normalization. For $\bar{E}_\gamma$ the difference is 0.9 MeV for ^{87}Br, 1.7 MeV for ^{88}Br, and 2.3 MeV for ^{94}Rb. The uncertainty quoted on the TAGS average energies in Table II is systematic since the contribution of statistical uncertainties in the case of $I_{\beta\gamma}(E_x)$ is negligible. The values of $\bar{E}_\gamma$ and $\bar{E}_\beta$ were computed for each intensity distribution that was used to define the space of accepted solutions in Fig. 5, and the maximum positive and negative differences with respect to the adopted solution are the values quoted in the table.

Table III shows the $\bar{E}_\beta$ given in Ref. [38] obtained from the β spectrum measurements of Tengblad *et al.* [37]. For comparison, the average β energy obtained from the present TAGS data, given in Table II, is incremented with the average β energy corresponding to the β-delayed neutron branch. The

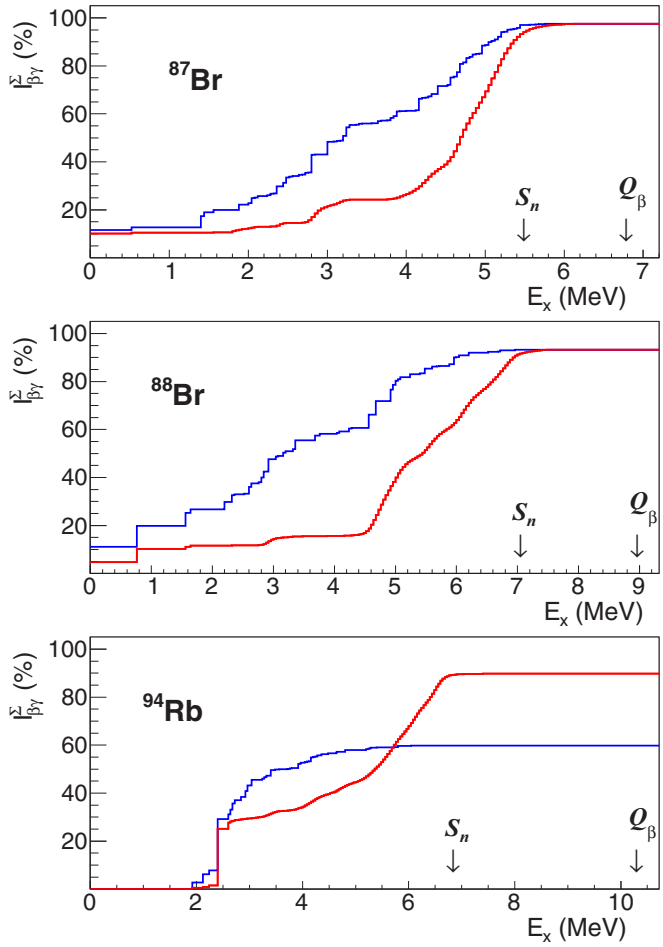

FIG. 6. Accumulated β-intensity distribution $I^{\Sigma}_{\beta\gamma}$: TAGS result (red line) and high-resolution measurements (blue line).

contribution of the βn branch is calculated from the $I_{\beta n}(E_x)$ distribution obtained as explained in Sec. II. We find that the values of Ref. [38] agree with our result for ^{88}Br but differ by 240 keV for ^{87}Br and 380 keV for ^{94}Rb. This situation is comparable to that observed for Greenwood *et al.* [12] TAGS data. Figure 7 presents in a graphical way the difference of average β energies $\Delta\bar{E}_\beta$ between the results of Tengblad *et al.* and the results of both Greenwood *et al.* and ourselves. In the figure, the differences are represented as a function of Q_β

TABLE II. Average γ and β energies calculated using $I_{\beta\gamma}(E_x)$-intensity distributions from ENSDF [1–3] and the present TAGS data. The contribution of the β-delayed neutron branch is not included. Note that the ENSDF values for ^{94}Rb are obtained with a β-intensity normalization of 59.8% (see text for details).

Isotope	$\bar{E}_\gamma$ (keV)		$\bar{E}_\beta$ (keV)	
	ENSDF	TAGS	ENSDF	TAGS
^{87}Br	3009	3938^{+40}_{-67}	1599	1159^{+32}_{-19}
^{88}Br	2892	4609^{+78}_{-67}	2491	1665^{+32}_{-38}
^{94}Rb	1729	4063^{+62}_{-66}	2019	2329^{+32}_{-30}

TABLE III. Comparison of average β energies obtained from direct β-spectrum measurement (Tengblad *et al.* [38]) with those obtained combining $I_{\beta\gamma}(E_x)$ from present TAGS data and $I_{\beta n}(E_x)$ derived from neutron spectrum data. See text for details.

Isotope	$\bar{E}_\beta$ (keV)	
	This work	Ref. [38]
^{87}Br	1170^{+32}_{-19}	1410 ± 10
^{88}Br	1706^{+32}_{-38}	1680 ± 10
^{94}Rb	2450^{+32}_{-30}	2830 ± 70

to illustrate what seems to be a systematic trend. Although the scattering of values is relatively large, on average the differences are smaller below ~5 MeV. The isotopes from Ref. [12] shown in Fig. 7 are ^{146}Ce, ^{145}Ce, ^{144}Ba, ^{141}Ba, ^{143}La, ^{94}Sr, ^{93}Sr, ^{145}La, ^{143}Ba, ^{89}Rb, ^{141}Cs, ^{145}Ba, ^{91}Rb, ^{95}Sr, ^{140}Cs, ^{90}Rb, ^{90m}Rb, and ^{93}Rb, in order of increasing Q_β.

More illustrative than the comparison of average values is the comparison of β-energy distributions $S_\beta(E_\beta)$ as is done in Fig. 8. Large differences in shape between the results of Tengblad *et al.* and the present TAGS results are clearly seen, even for ^{88}Br, where the average values agree. The contribution of the β-delayed neutron branch, added to the TAGS result for the comparison, is shown. This contribution is calculated using the $I_{\beta n}(E_x)$ distribution obtained from the deconvolution of the known neutron spectrum (see Sec. II). For reference, we also include in the figure the distribution calculated from the HRGS level scheme in ENSDF. The $S_\beta(E_\beta)$ distribution calculated from the TAGS data is shifted to lower energies for the three isotopes, in comparison to the direct β-spectrum measurement. We should point out that a similar trend is found for the remaining isotopes included in the same experimental campaign, ^{86}Br and ^{91}Rb [80] and ^{92,93}Rb [36,65], where we find deviations in $\Delta\bar{E}_\beta$ in the range 200 to 400 keV. Moreover, our results for ^{91}Rb and ^{93}Rb agree rather well with those obtained by Greenwood *et al.* [12].

The assumption of an allowed shape used here to calculate $S_\beta(E_\beta)$ from $I_\beta(E_x)$ introduces some uncertainty in the comparison. However, it is likely to be a good approximation.

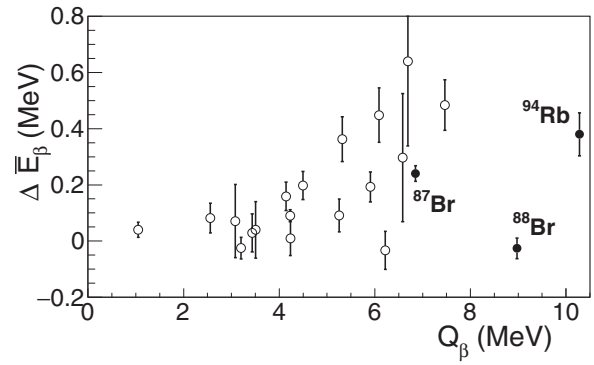

FIG. 7. Difference between average β energies obtained by direct β spectrum measurements (Tengblad *et al.* [38]) and from TAGS β-intensity distributions. TAGS results are from Ref. [12] (open circles) and from the present work (filled circles).

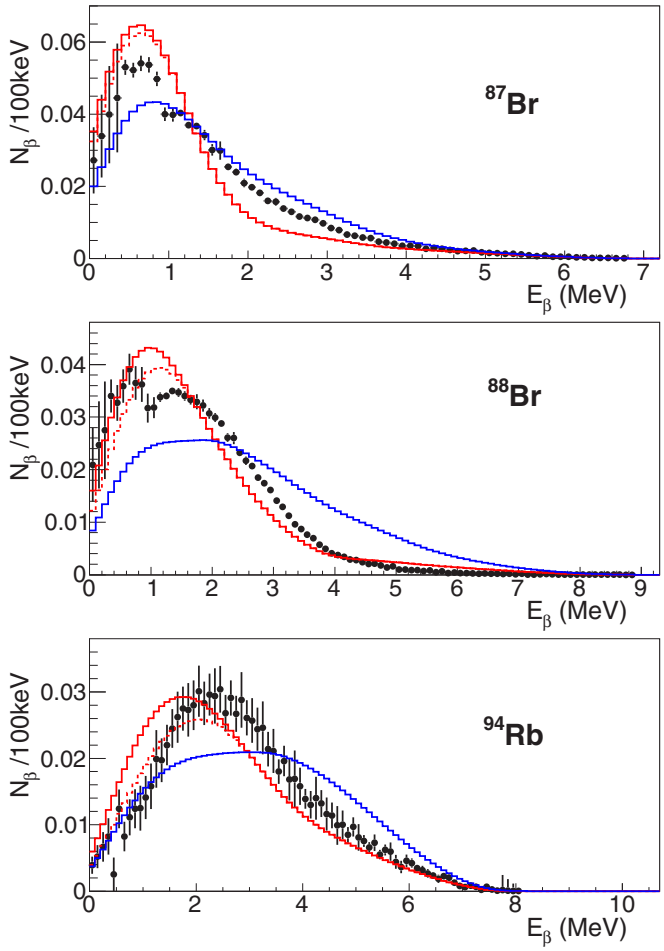

FIG. 8. Comparison of β spectra S_β. Tengblad *et al.* [38]: black circles; present TAGS result: dashed red line; present TAGS plus β delayed neutron contribution: continuous red line; high-resolution measurements [1–3]: blue line.

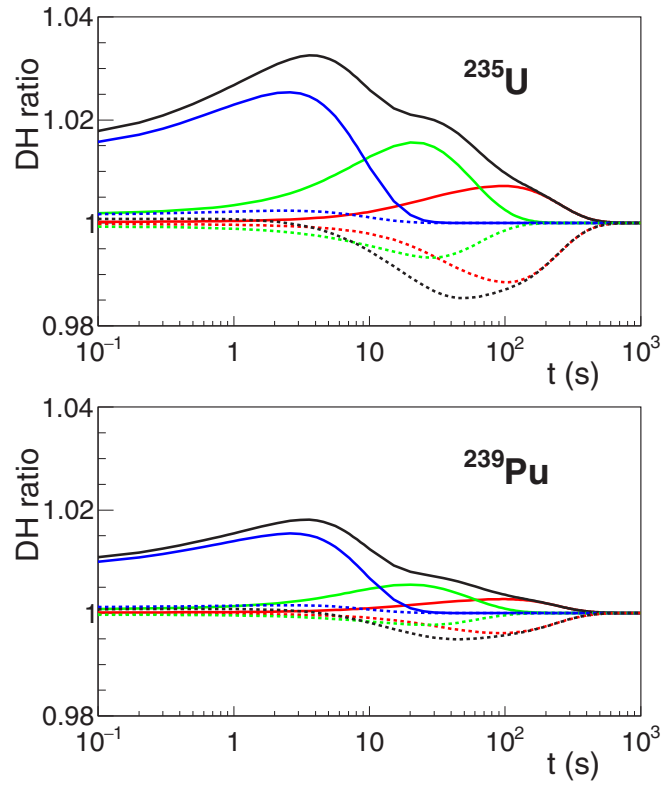

FIG. 9. Ratio of decay heat as a function of cooling time calculated for ^{235}U and ^{239}Pu when our TAGS data replace high-resolution data. Continuous line: photon component; dashed line: electron component. Red: ^{87}Br; green: ^{88}Br; blue: ^{94}Rb; black: all three isotopes.

Thus to explain the difference between TAGS results and the direct β-spectrum measurement one is forced to consider systematic errors in the use of either one of the two techniques or both. As explained above, we investigated carefully sources of systematic uncertainty, which can lead to distortions of the β-energy distribution and found that none of them can explain the observed differences (see Table III). Moreover, as shown in Fig. 5, the measured TAGS spectrum imposes a strong constraint on the bulk of the β-intensity distribution. It is difficult to imagine additional sources of systematic uncertainty, which can have a significant impact on the shape of this distribution. To clarify the discrepancy, new measurements of the spectrum of β particles emitted in the decay of a number of selected isotopes would be of great value.

To finalize this part of the discussion we should point out that $\bar{E}_\gamma$ can be obtained from the β spectra measured in Ref. [37]. This can be achieved by deconvolution of the β spectra with appropriate β shapes $s_\beta(Q_\beta - E_x, E)$ to obtain the $I_\beta(E_x)$ [see Eq. (4)]. As a matter of fact, this procedure is needed (and applied in Ref. [37]) to obtain the antineutrino spectrum using Eq. (3). The average γ energies obtained in this way would show systematic differences with respect to TAGS results of opposite sign to those found for $\bar{E}_\beta$. Rather than using this approach, the authors of Ref. [38] determine average γ energies $\bar{E}_\gamma$ from an independent set of measurements using a NaI(Tl) detector to obtain the spectrum of γ rays for the decay of each isotope. There are also large discrepancies between these results and those obtained from TAGS measurements. We postpone the discussion of these differences to a forthcoming publication [80].

The impact of the present TAGS results for $\bar{E}_\gamma$ and $\bar{E}_\beta$ on decay-heat summation calculations was evaluated. Figure 9 shows the ratio of calculations using TAGS data to calculations using HRGS data. The figure shows the evolution of the ratio as a function of cooling time following the prompt thermal fission of ^{235}U and ^{239}Pu. Both together account for most of the power released in most reactors. The calculation is similar to that described in Ref. [35]. It uses fission yields from JEFF-3.1 [81] and the ENDF/B-VII updated decay data sublibrary. The update introduces β-intensity distributions from previous TAGS measurements and, for a few isotopes, from β-spectrum measurements and from theoretical calculations. In the cases of ^{87}Br, ^{88}Br, and ^{94}Rb, the database adopts the ENSDF average γ and β energies from HRGS (Table II). As is customary the DH is evaluated separately for the electromagnetic energy (EEM), or photon component (γ rays, x rays), and for the light particle energy (ELP) or electron component (β particles, conversion electrons, Auger electrons). The ratio is computed

for each individual isotope and for the three isotopes together. As expected, the effect of the inclusion of TAGS data is largest for ^{94}Rb and smallest for ^{87}Br. The largest variation in the EEM component occurs at short cooling times between 1 and 10 s. Due to the particular normalization of the high-resolution ^{94}Rb β-intensity distribution mentioned above, the effect is not observed in the ELP component (see also Table II). The effect is larger for ^{235}U fission, due to the larger fission yields for the three isotopes, reaching an increment of 3.3% for the combined contribution to the EEM component at $t = 3.5$ s. For ^{239}Pu the increment reaches 1.8%. Although the impact is somewhat small, the present data contribute to reduce the discrepancy between DH integral measurements and summation calculations for ^{235}U in the range of 1 to 100 s (see, for example, Fig. 12 of Ref. [82]).

V. ANTINEUTRINO SPECTRA

The impact of our data on calculated antineutrino spectrum is shown in Figs. 10 and 11. The $\bar{\nu}_e$ summation calculation of Fig. 10 is analogous to the DH calculation of Fig. 9. It shows for ^{235}U and ^{239}Pu fission the ratio of calculated $\bar{\nu}_e$ spectrum when our TAGS data replace HRGS data. The effect of each individual isotope and of the three together is shown. For both fissioning systems the impact of ^{87}Br is negligible, while the effect of ^{88}Br peaks around 8.5 MeV (3%) and that of ^{94}Rb peaks around 7 MeV (4%). The combined effect is

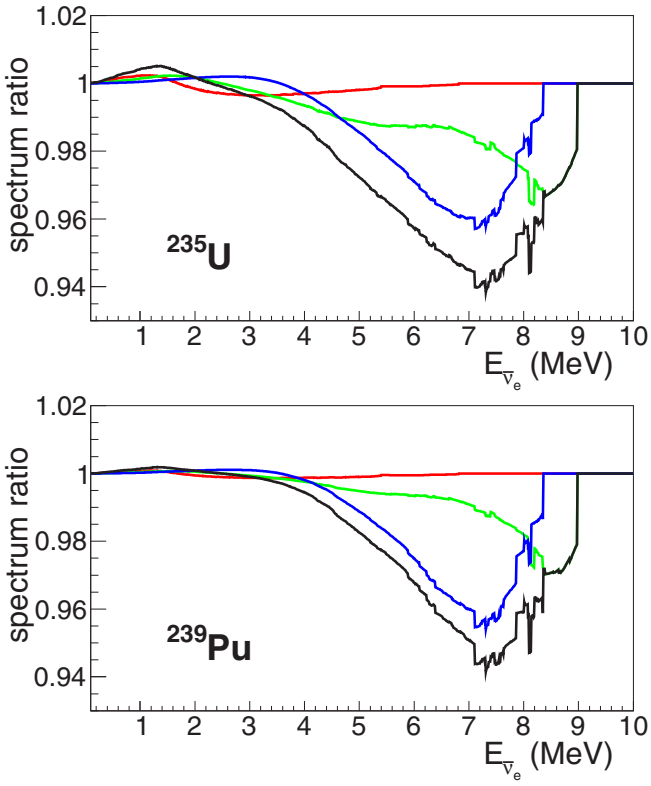

FIG. 10. Ratio of antineutrino spectra as a function of energy calculated for ^{235}U and ^{239}Pu when our TAGS data replace high-resolution data. Red: ^{87}Br; green: ^{88}Br; blue: ^{94}Rb; black: all three isotopes.

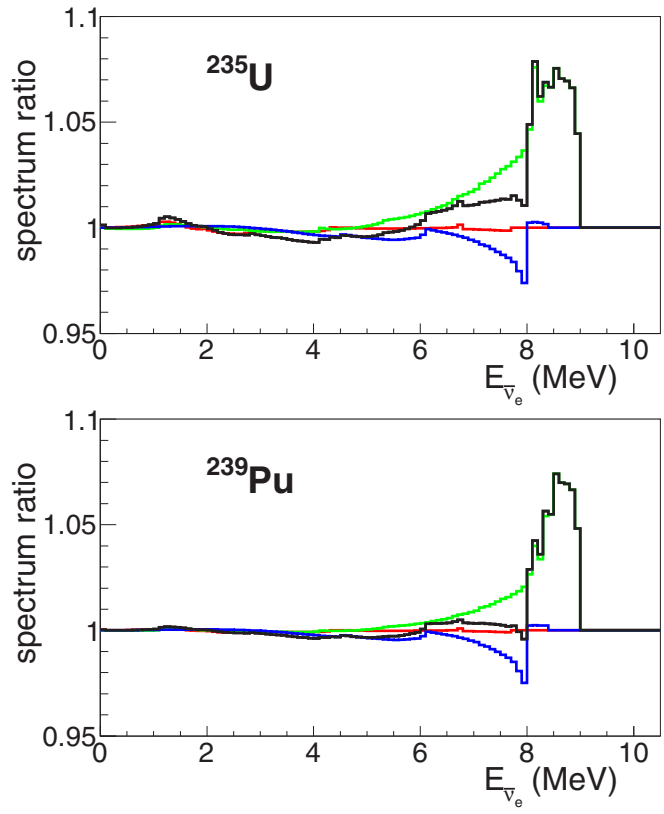

FIG. 11. Ratio of antineutrino spectra as a function of energy calculated for ^{235}U and ^{239}Pu when our TAGS data replace the data of Tengblad *et al.* Red: ^{87}Br; green: ^{88}Br; blue: ^{94}Rb; black: all three isotopes.

a reduction of the calculated $\bar{\nu}_e$ spectrum, which reaches a value of 6% around 7.2 MeV. Similar figures are obtained for ^{238}U and ^{241}Pu. It is remarkable that the effect of our TAGS data for ^{88}Br and ^{94}Rb is of equal importance to that of the combined effect of recently measured [83] TAGS data for ^{92}Rb, ^{96}Y, and ^{142}Cs. Compare Fig. 10 in the present work with Fig. 6 of Ref. [83], which shows an effect of similar shape and magnitude. These three isotopes contribute most to the $\bar{\nu}_e$ spectrum around 7 MeV, with ^{92}Rb being the largest contributor [36]. Due to current uncertainties in the summation method, it is not easy to draw conclusions on the impact of both experiments on the origin of the antineutrino spectrum shape distortion. Note that they lead to a *reduction* of the calculated spectrum, which is maximum about 1 MeV above the center of the observed *excess*. Better quality data for a larger set of isotopes, including decay data and fission yields, are required. Our result shows the importance of performing TAGS measurements for fission products with very large Q_β value, which are likely to be affected by large Pandemonium systematic error, even if they have moderate fission yields.

Figure 11 shows a different set of $\bar{\nu}_e$ summation calculations. The calculation is analogous to that described in Ref. [29]. It uses a different selection of decay data from the calculation shown in Fig. 10. More specifically, it uses antineutrino spectra derived from the β spectra of Tengblad *et al.* [37] for ^{87,88}Br and ^{94}Rb instead of $\bar{\nu}_e$ spectra derived

from high-resolution data. Thus Fig. 11 shows the effect of replacing Tengblad *et al.* data with our TAGS data. As can be seen, the replacement of ^{87}Br has little impact, while there is a cancellation below $E_{\bar{\nu}_e} = 8$ MeV between the ^{88}Br and ^{94}Rb deviations. However, the difference between our TAGS data and the data of Tengblad *et al.* for ^{88}Br produces an increase in the calculated antineutrino spectra of about 7% between 8 and 9 MeV. Note that although ^{94}Rb has a Q_β of 10.28 MeV we do not observe appreciable β intensity below 2.41 MeV excitation energy, and thus the maximum effective endpoint energy is below 8 MeV. The relatively large impact of ^{88}Br is due to the fact that only a few decay branches contribute to the spectrum here. Note that in this energy interval the uncertainty of the integral β-spectrum measurements [21,22] is relatively large, and thus summation calculations are particularly relevant. This points again to the need to perform TAGS measurements for fission products with very large Q_β.

VI. γ INTENSITY FROM NEUTRON UNBOUND STATES

Figure 4 shows for all three isotopes a sizable TAGS intensity $I_{\beta\gamma}(E_x)$ above S_n. This intensity extends well beyond the first few hundred keV, where the low neutron penetrability makes γ-ray emission competitive. For comparison, the figure includes the β-intensity distribution followed by neutron emission $I_{\beta n}(E_x)$ deduced from the neutron spectrum as explained above. The integrated decay intensity above S_n followed by γ-ray emission $P_\gamma = \int_{S_n}^{Q_\beta} I_{\beta\gamma}(E_x)dE_x$ obtained from the TAGS measurement is compared to the integrated $I_{\beta n}(E_x)$ or P_n value in Table IV. Surprisingly large values of P_γ are obtained, which in the case of ^{87}Br is even larger than P_n. The γ branching represents 57% of the total for ^{87}Br, 20% for ^{87}Br, and 4.5% for ^{94}Rb. In the case of ^{87}Br we find 8 times more intensity than the high-resolution experiment [50], which can be explained by the Pandemonium effect. The quoted uncertainty on the TAGS integrated intensity P_γ is completely dominated by systematic uncertainties since the uncertainty due to data statistics is below 0.6% (relative value) in all cases.

We have evaluated several sources of systematic uncertainty. In the first place we consider uncertainties that affect the overall β-intensity distributions, which were already detailed in Sec. III. To quantify the uncertainties in P_γ coming from the spread of possible solutions compatible with the data (see Fig. 5), we follow the approach used in Sec. IV and take the maximum positive and negative differences with respect to the adopted solution as a measure of this uncertainty.

In addition to this, we consider other sources of uncertainty which mostly affect the integral value.

TABLE IV. Integrated β-intensity P_γ from TAGS data above S_n compared to P_n values from Refs. [1–3].

Isotope	P_γ (%)	P_n (%)
^{87}Br	3.50^{+49}_{-40}	2.60(4)
^{88}Br	1.59^{+27}_{-22}	6.4(6)
^{94}Rb	0.53^{+33}_{-22}	10.18(24)

A possible source of uncertainty is related to the correlations introduced by the finite-energy resolution in the deconvolution process. This can cause a relocation of counts in a region of rapidly changing intensity [73], such as the region around S_n. However, we estimate from a model deconvolution that this effect is not relevant in the present case. Likewise the uncertainty on width calibration also has an impact on the redistribution of counts around S_n. The highest width calibration point is at 4.123 MeV. From the comparison of different fits, varying the number and distribution of calibration points, we determine that the extrapolation of the calibration curve can vary by up to $\pm$15% at 10 MeV. This introduces an uncertainty in P_γ of 2% for ^{87}Br and 6% for ^{88}Br and ^{94}Rb.

The uncertainty in the energy calibration of TAGS spectra might have an impact on the result because of the dependence of the response on energy. However, we verified that this effect is negligible. The main effect of the uncertainty on the energy calibration is on the integration range. Since the intensity is rapidly changing in the region around S_n the effect can be large. The fact that the structure observed in the distribution of Fig. 12 around 7–8 MeV for ^{94}Rb coincides with the levels populated in the final nucleus (see next section) allows us to

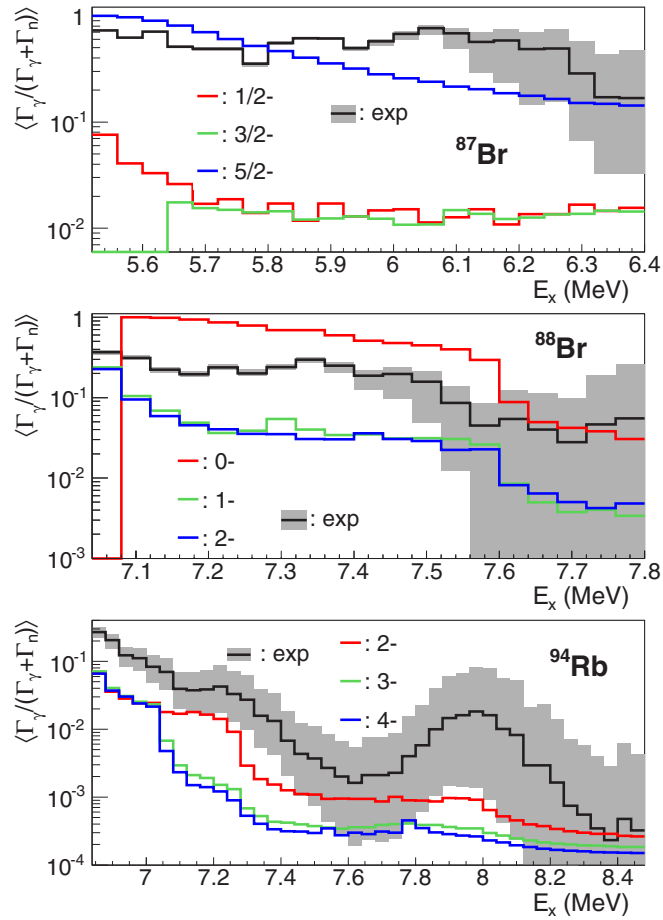

FIG. 12. Average γ to total width from experiment (black line) and calculated for the three spin-parity groups populated in allowed decay (red, green, blue). The gray-shaded area around the experiment indicates the sensitivity to systematic effects. See text for details.

conclude that the energy calibration at S_n is correct to about one energy bin (40 keV). We evaluate the uncertainty in the integral, equivalent to changes of half a bin, to be 11% for the bromine isotopes and 15% for rubidium.

The uncertainty values entered in Table IV correspond to the sum in quadrature of the three types of uncertainty mentioned above: uncertainties in the deconvolution, and uncertainties in the resolution and energy calibration.

VII. COMPARISON WITH HAUSER-FESHBACH CALCULATIONS

We show in Fig. 12 the ratio $I_{\beta\gamma}(E_x)/[I_{\beta\gamma}(E_x) + I_{\beta n}(E_x)]$ as a function of excitation energy. The shaded area represents the uncertainty in the ratio coming from the spread of solutions $I_{\beta\gamma}(E_x)$ to the TAGS inverse problem shown in Fig. 5. It should be noted that the ratio is affected also by systematic uncertainties in the $I_{\beta n}(E_x)$ distribution coming from the deconvolution of neutron experimental spectra as well as by uncertainties in the neutron spectra themselves, but they are not considered here.

The experimental intensity ratio in Fig. 12 is identical to the average ratio $\langle \Gamma_\gamma(E_x)/\,\Gamma_{\rm tot}(E_x)\rangle$. The average is taken over all levels in each bin populated in the decay. Thus the experimental distribution can be directly compared with the results of Hauser-Feshbach calculations of this ratio. The NLD and PSF used in the calculations are the same as used to construct the spectrometer response to the decay (see Sec. III). The new ingredient needed is the NTC, which is obtained from the optical model (OM). It is calculated with Raynal's ECIS06 OM code integrated in the TALYS-1.4 software package [84]. OM parameters are taken from the so-called local parametrization of Ref. [85]. Neutron transmission is calculated for final levels known to be populated in the decay: ground state of ^{86}Kr, ground state and first excited state of ^{87}Kr, and ground state plus 8 excited states of ^{93}Sr. With these ingredients, one obtains the average widths $\langle\Gamma_\gamma\rangle$ and $\langle\Gamma_n\rangle$ (see the appendix).

In the case of ^{87}Kr we can compare the calculated average values with experimental data obtained from neutron capture and transmission reactions [50,62], in particular, for $1/2^-$ and $3/2^-$ resonances which are populated in the decay of a $3/2^-$ ^{87}Br ground state. Up to 50 $1/2^-$ and 66 $3/2^-$ resonances were identified in an interval of 960 keV above S_n. The NLD of Ref. [75] predicts 46 and 90, respectively, in fair agreement with these values. The distribution of neutron widths for $1/2^-$ resonances in the interval $E_n = 250$–960 keV is compatible with a PT distribution with average width $\langle\Gamma_n\rangle = 1.95$ keV. The same is true for $3/2^-$ resonances with $\langle\Gamma_n\rangle = 2.79$ keV. In the same interval, the Hauser-Feshbach calculated widths vary between 0.3 and 0.7 keV for $1/2^-$ states and between 0.5 and 0.9 keV for $3/2^-$ states. In both cases, the calculation is about four times too low. The information on $\langle\Gamma_\gamma\rangle$ is less abundant. The γ width has been determined for six $1/2^-$ and ten $3/2^-$ resonances, with values in the range 0.075–0.48 eV, and is fixed to 0.255 eV, from systematics, for the remaining resonances. The Hauser-Feshbach calculation gives values in the range 0.08–0.12 eV. On average, the calculation is about a factor of 3 too low. Since the NLD reproduces the number of resonances, to reach such values for the partial widths requires a renormalization by a factor of 3–4 for the PSF and the NTC in ^{87}Kr, which seems large. The reader should note that variations of similar magnitude and direction for both the PSF and NTC have little impact on the calculated ratio $\langle\Gamma_\gamma/\,\Gamma_{\rm tot}\rangle$. It should also be noted that this ratio is insensitive to changes in NLD.

We show in Fig. 12 the ratio $\langle\Gamma_\gamma/\,\Gamma_{\rm tot}\rangle$, calculated with nuclear statistical parameters as described above, for the three spin-parity groups populated under the Gamow-Teller selection rule. Due to statistical fluctuations affecting individual widths [61], this cannot be obtained as $\langle\Gamma_\gamma\rangle/(\langle\Gamma_\gamma\rangle + \langle\Gamma_n\rangle)$. Rather than trying to obtain a formula for the average correction factor to be applied to this ratio, which is the common practice for cross section calculations [84], we use the Monte Carlo method to obtain directly the average of width ratios. The procedure to obtain a statistical realization (or sample) from the model is similar to that described in Ref. [72]. Level energies for each spin parity are generated according to a Wigner distribution from the NLD. For each state, the corresponding Γ_γ and Γ_n to individual final states are sampled from PT distributions with the calculated average values (see the appendix). The total γ and neutron widths are obtained by summation over all possible final states and the ratio is computed. The ratio is averaged for all levels lying within each energy bin (40 keV). In order to eliminate fluctuations in the calculated averages, the procedure is repeated between 5 and 1000 times depending on level density. Very large average enhancement factors are obtained, reaching two orders of magnitude, when the neutron emission is dominated by the transition to a single final state.

In the case of the decay of the $3/2^-$ ground state in ^{87}Br, one can see in Fig. 12 that the strong γ-ray emission above S_n can be explained as a consequence of the large hindrance of $l = 3$ neutron emission from $5/2^-$ states in ^{87}Kr to the 0^+ ground state of ^{86}Kr. This is the explanation already proposed in Ref. [50]. The situation is even more favorable to this explanation if the spin parity of ^{87}Br were $5/2^-$ as suggested in Ref. [76]. In this case, the neutron emission is hindered for both $5/2^-$ and $7/2^-$ states populated in the allowed decay. In the case of ^{88}Br 1^- decay a similar situation occurs for 0^- states in ^{88}Kr below the first excited state in ^{87}Kr at 532 keV, which requires $l = 3$ neutron emission to populate the $5/2^+$ ground state in ^{87}Kr. It should be noted that if the spin parity of ^{88}Br were 2^- as suggested in Ref. [2], the three allowed spin-parity groups (1^-,2^-,3^-) will have similar γ-to-total ratios, a factor of 3 to 5 too low compared to experiment, which reinforces our choice of 1^- for the ^{88}Br ground state. A more quantitative comparison of the experimental and calculated ratios requires a knowledge of the distribution of β intensity between the three spin groups. This can be obtained from β-strength theoretical calculations, such as those in Ref. [86], for example. It is clear, however, that for both bromine isotopes the large γ branching above S_n can be explained as a nuclear structure effect: the absence of states in the final nucleus which can be populated through the emission of neutrons of low orbital angular momentum.

The case of ^{94}Rb 3^- decay is the most interesting. The final nucleus ^{93}Sr is five neutrons away from β stability. Although the γ intensity is strongly reduced, only 5% of

the neutron intensity is detectable up to more than 1 MeV above S_n. The structure observed in the distribution of the average ratio $\langle \Gamma_\gamma / \Gamma_{\rm tot} \rangle$ can be associated with the opening of βn channels to different excited states in ^{93}Sr. As can be seen, the structure is reproduced by the calculation, which confirms the energy calibration at high excitation energies. In any case the calculated average γ-to-total ratio is well below the experimental value. In order to bring the calculation in line with the experimental value one would need to enhance the γ width, or suppress the neutron width, or any suitable combination of the two, by a very large factor of about one order of magnitude. A large enhancement of the γ width, and thus of the calculated (n,γ) cross sections, would have an impact on r-process abundance calculations [42–44]. It would be necessary to confirm the large enhancement of the $\langle \Gamma_\gamma / \Gamma_{\rm tot} \rangle$ ratio observed in ^{94}Rb with similar studies on other neutron-rich nuclei in this mass region as well as in other mass regions. It will also be important to quantify the contribution of a possible suppression of the neutron width to the observed ratio.

VIII. SUMMARY AND CONCLUSION

We apply the TAGS technique to study the decay of three β-delayed neutron emitters. For this we use a new segmented BaF_2 spectrometer with reduced neutron sensitivity, which proved to be well suited to this purpose. The three isotopes, ^{87}Br, ^{88}Br, and ^{94}Rb, are fission products with impact in reactor decay heat and antineutrino spectrum summation calculations. We obtain β-intensity distributions which are free from the Pandemonium systematic error, affecting the data available in the ENSDF database for the three isotopes. The average γ-ray energies that we obtain are 31%, 59%, and 235% larger than those calculated with this database for ^{87}Br, ^{88}Br, and ^{94}Rb respectively, while the average β energies are 28%, 33%, and 13% smaller.

We compare the energy distribution of β particles emitted in the decay derived from our β-intensity distributions with the direct β-spectrum measurement performed by Tengblad *et al.* and find significant discrepancies. Our distributions are shifted to somewhat lower energies. This is reflected in the average β energies, which we find to be 17% and 13% smaller for ^{87}Br and ^{94}Rb respectively. Similar systematic differences are found when the TAGS data of Greenwood *et al.* for 18 isotopes is compared with the data of Tengblad *et al.* We performed a thorough investigation of possible systematic errors in the TAGS technique and found that none of them can explain the observed differences. It will be important to perform new direct measurements of the β spectrum for a few selected isotopes in order to investigate this issue further.

We estimate the effect of the present data on DH summation calculations. We find a relatively modest impact when the high-resolution decay data are replaced by our TAGS data. The impact in the photon component is largest at short cooling times. For ^{235}U thermal fission, it reaches an increment of 3.3% around 3.5 s after fission termination. This is mainly due to the decay of ^{94}Rb. The influence of ^{88}Br is smaller and peaks at around 25 s. In spite of being small, it contributes to reduce the discrepancy between DH integral measurements of the EEM component and summation calculations for ^{235}U in the range of 1 to 100 s. Many FP contribute in this time range, and thus additional TAGS measurements of short-lived FP are required to remove the discrepancy. In the case of ^{239}Pu the maximum increment is about 1.8%.

We also evaluate the impact of the new TAGS data on antineutrino spectrum summation calculations. When our data replace the data from high-resolution measurements, we observe a reduction of the calculated $\bar{\nu}_e$ spectrum, which reaches a maximum value of 6% at 7 MeV for the thermal fission of ^{235}U. A similar value is obtained for ^{239}Pu. The reduction is mainly due to the decay of ^{94}Rb. The effect of ^{88}Br, somewhat smaller, peaks at 8.5 MeV. It is remarkable that we find an impact similar to that observed recently for ^{92}Rb, ^{96}Y, and ^{142}Cs together, which make the largest contribution to the antineutrino spectrum at these energies. The reason is that the large value of the Pandemonium systematic error prevails over the relatively small fission yield for the isotopes studied in the present work. We also verified the effect of replacing our TAGS data with Tengblad *et al.*'s β-spectrum data. We found a relatively small impact below $E_{\bar{\nu}_e} = 8$ MeV, in part due to a compensation effect of the deviations for ^{94}Rb and ^{88}Br. However, between 8 and 9 MeV the use of TAGS data for ^{88}Br leads to an increase of about 7% in the calculated antineutrino spectrum. This relatively large impact is due to the small number of decay branches in this energy range. All this underlines the need for TAGS measurements for fission products with a very large Q_β decay energy window.

We confirm the suitability of the TAGS technique for obtaining accurate information on γ-ray emission from neutron-unbound states. In order to assess the reliability of the result we examined the systematic errors carefully since they dominate the total uncertainty budget. Surprisingly large γ-ray branchings of 57% and 20% were observed for ^{87}Br and ^{88}Br respectively. In the case of ^{94}Rb, the measured branching of 4.5% is smaller but still significant. For ^{87}Br we observe 8 times more intensity than previously detected with high-resolution γ-ray spectroscopy, which confirms the need to use the TAGS technique for such studies.

Combining the information obtained from TAGS measurements about the γ intensity from states above S_n with the β-delayed neutron intensity, we can determine the branching ratio $\langle \Gamma_\gamma/(\Gamma_\gamma + \Gamma_n) \rangle$ as a function of E_x. The information thus acquired can be used to constrain the neutron-capture cross section for unstable neutron-rich nuclei. This opens a new field for applications of β-decay TAGS studies. It also provides additional arguments for the need for accurate measurements of β-delayed neutron emission in exotic nuclei. The measurements should cover neutron spectra and yields as well as neutron-γ coincidences.

From the comparison of our experimental results with Hauser-Feshbach calculations, we conclude that the large γ branching observed in ^{87}Br and ^{88}Br is a consequence of the nuclear structure. Some of the resonances populated in the decay can only disintegrate via the emission of a kinematically hindered neutron to the levels available in the final nucleus. A similar situation can occur for other β-delayed neutron emitters, when the number of levels in the final nucleus within the emission window $Q_\beta - S_n$ is small. It should be noted

that such strong γ to neutron competition introduces a large correction to the estimation of β-delayed neutron emission probabilities from β-strength calculations and should be taken into account when comparing experiment with calculation.

The case of ^{94}Rb is more representative of the situation expected for nuclei far from stability, where many levels are available, and thus the decay by low l neutron emission is always possible. For ^{94}Rb we find that the γ-ray emission from neutron-unbound states is largely suppressed, but still much larger (an order of magnitude) than the result of Hauser-Feshbach calculations using standard parameters for level density, photon strength, and neutron transmission. If such enhancement with respect to the Hauser-Feshbach model is due mainly to an increment in the radiative width, then a similar increase is obtained for the neutron-capture cross section. This can have a significant impact on calculated elemental abundances in the astrophysical r-process. It is necessary to confirm and generalize the result obtained for the neutron-rich nucleus ^{94}Rb extending this type of study to other β-delayed neutron emitters in the same and different mass regions, in particular farther away from the valley of β stability. Such measurements using the TAGS technique are already under way and additional studies are planned.

Note added in proof. In a recent publication [87], following our original work [9], the TAGS technique has been applied to study the decay of the ^{70}Co $(6,7)^-$ isomer and the authors of this work report large γ intensities from states above S_n. The integrated $I_{\beta\gamma}(E_x)$ is about 12.5%, certainly much larger than those observed in our work. Since the P_n value is not known, the γ-to-total branching could not be determined. Nevertheless the authors find that a strong suppression of neutron emission can be expected for this decay from the small overlap between initial and final state wave functions. Whether the same mechanism can explain the discrepancies we observe for ^{94}Rb between experiment and Hauser-Feshbach calculations remains to be explored.

ACKNOWLEDGMENTS

This work was supported by Spanish Ministerio de Economía y Competitividad under Grants No. FPA2008-06419, No. FPA2010-17142, No. FPA2011- 24553, No. FPA2014-52823-C2-1-P, and No. CPAN CSD-2007-00042 (Ingenio2010) and the program Severo Ochoa (SEV-2014-0398). W.G. would like to thank the University of Valencia for support. This work was supported by the Academy of Finland under the Finnish Centre of Excellence Programme 2012–2017 (Project No. 213503, Nuclear and Accelerator-Based Physics Research at JYFL). Work was also supported by EPSRC (UK) and STFC (UK). Work was partially supported by the European Commission under FP7/EURATOM Contract No. 605203. F.G.K. acknowledges support from the U.S. Department of Energy, under Contract No. DE-AC02-06CH11357. We thank David Lhuillier for making available in digital form the data tabulated in Ref. [38]. The authors would like to thank the late Olivier Bersillon for drawing our attention to the inconsistencies between average decay energies obtained from Refs. [38] and [12].

APPENDIX

The average γ width for initial levels (resonances) of spin parity J_i^π at excitation energy E_x can be obtained by summation over all final states of spin parity J_f^π and excitation energy $E_x - E_\gamma$:

$$\langle\Gamma_\gamma(J_i^\pi,E_x)\rangle = \sum_f \langle\Gamma_\gamma(J_i^\pi,E_x,E_\gamma)\rangle = \frac{1}{\rho(J_i^\pi,E_x)}\sum_f\sum_{XL} E_\gamma^{2L+1}\mathrm{f}_{XL}(E_\gamma), \quad \text{(A1)}$$

where $\rho(J_i^\pi,E_x)$ represents the density of initial levels and $\mathrm{f}_{XL}(E_\gamma)$ is the photon strength for transition energy E_γ. The appropriate electric or magnetic character X and multipolarity L of the transition is selected by spin and parity conservation. We have used the common practice of restricting the transition types to $E1$, $M1$, and $E2$ with no mixing, which leads to a single XL choice for each final state.

For transitions into a bin of width ΔE in the continuum part of the level scheme, the density-weighted average over final levels should be used:

$$\langle\Gamma_\gamma(J_i^\pi,E_x)\rangle = \frac{1}{\rho(J_i^\pi,E_x)}\sum_f\sum_{XL}\int_E^{E+\Delta E} E_\gamma^{2L+1} \times \mathrm{f}_{XL}(E_\gamma)\rho(J_f^\pi,E_x-E_\gamma)\,dE_\gamma. \quad \text{(A2)}$$

Likewise, the average neutron width can be obtained by summation over all final states of spin parity J_f^π and excitation energy $E_x - S_n - E_n$ in the final nucleus:

$$\langle\Gamma_n(J_i^\pi,E_x)\rangle = \sum_f \langle\Gamma_n(J_i^\pi,E_x,E_n)\rangle = \frac{1}{2\pi\rho(J_i^\pi,E_x)}\sum_f\sum_{ls} T^{ls}(E_n), \quad \text{(A3)}$$

where $T^{ls}(E_n)$ is the neutron transmission coefficient, a function of neutron energy E_n. The orbital angular momentum l and channel spin s are selected by spin and parity conservation for each final level.

The average over initial spin parities J_i^π at each E_x is obtained using the corresponding weights $w(J_i^\pi,E_x)$, properly normalized $\sum_i w(J_i^\pi,E_x) = 1$, from

$$\langle\Gamma_\gamma(E_x)\rangle = \sum_i w(J_i^\pi,E_x)\langle\Gamma_\gamma(J_i^\pi,E_x)\rangle, \quad \text{(A4)}$$

$$\langle\Gamma_n(E_x)\rangle = \sum_i w(J_i^\pi,E_x)\langle\Gamma_n(J_i^\pi,E_x)\rangle. \quad \text{(A5)}$$

[1] R. G. Helmer, Nucl. Data Sheets **95**, 543 (2002).
[2] E. A. McCutchan and A. A. Sonzogni, Nucl. Data Sheets **115**, 135 (2014).
[3] D. Abriola and A. A. Sonzogni, Nucl. Data Sheets **107**, 2423 (2006).
[4] J. Hardy *et al.*, Phys. Lett. B **71**, 307 (1977).

[5] C. L. Duke *et al.*, Nucl. Phys. A **151**, 609 (1970).
[6] A. Algora *et al.*, Nucl. Phys. A **654**, 727c (1999).
[7] A. Algora *et al.* (GSI Euroball Collaboration), Phys. Rev. C **68**, 034301 (2003).
[8] Z. Hu *et al.*, Phys. Rev. C **60**, 024315 (1999).
[9] J. L. Tain *et al.*, Phys. Rev. Lett. **115**, 062502 (2015).
[10] K. Okumura *et al.*, in *Proceedings of the 2012 Symposium on Nuclear Data, Kyoto*, JAEA-Conf. 2013-002, INDC(JPN)-198 (Japan Atomic Energy Agency, Tokaimura, 2013), p. 15.
[11] T. Yoshida and R. Nakasima, J. Nucl. Sci. Technol. **18**, 393 (1981).
[12] R. C. Greenwood *et al.*, Nucl. Instrum. Methods Phys. Res., Sect. A **390**, 95 (1997).
[13] T. Yoshida *et al.*, *Assessment of Fission Product Decay Data for Decay Heat Calculations* (OECD/NEA Working Party for International Evaluation Co-operation, Paris, 2007), Vol. 25.
[14] M. Gupta *et al.*, Decay heat calculations: Assessment of fission product decay data requirements for Th/U Fuel, IAEA Report No. INDC(NDS)-0577, 2010 (unpublished).
[15] A. Algora *et al.*, Phys. Rev. Lett. **105**, 202501 (2010).
[16] M. Fleming and J. C. Sublet, Decay Data Comparisons for Decay Heat and Inventory Simulations of Fission Events, UK Atomic Energy Authority, Culham Science Centre, CCFE-R(15)28/S1, 2015 (unpublished).
[17] RIPL-3, R. Capote *et al.*, Nucl. Data Sheets **110**, 3107 (2009).
[18] C. Bemporad *et al.*, Rev. Mod. Phys. **74**, 297 (2002).
[19] S.-B. Kim *et al.*, Adv. High Energy Phys. **2013**, 453816 (2013).
[20] M. Cribier, Nucl. Phys. B (Proc. Suppl.) **221**, 57 (2011).
[21] K. Schreckenbach *et al.*, Phys. Lett. B **160**, 325 (1985).
[22] A. A. Hahn *et al.*, Phys. Lett. B **218**, 365 (1989).
[23] N. Haag, A. Gütlein, M. Hofmann, L. Oberauer, W. Potzel, K. Schreckenbach, and F. M. Wagner, Phys. Rev. Lett. **112**, 122501 (2014).
[24] T. A. Mueller, D. Lhuillier, M. Fallot, A. Letourneau, S. Cormon, M. Fechner, L. Giot, T. Lasserre, J. Martino, G. Mention, A. Porta, and F. Yermia, Phys. Rev. C **83**, 054615 (2011).
[25] P. Huber, Phys. Rev. C **84**, 024617 (2011).
[26] G. Mention, M. Fechner, T. Lasserre, T. A. Mueller, D. Lhuillier, M. Cribier, and A. Letourneau, Phys. Rev. D **83**, 073006 (2011).
[27] A. C. Hayes, J. L. Friar, G. T. Garvey, G. Jungman, and G. Jonkmans, Phys. Rev. Lett. **112**, 202501 (2014).
[28] D. L. Fang and B. A. Brown, Phys. Rev. C **91**, 025503 (2015),
[29] M. Fallot *et al.*, Phys. Rev. Lett. **109**, 202504 (2012).
[30] Y. Abe *et al.*, J. High Energy Phys. 10 (2014) 086.
[31] J. H. Choi *et al.*, Phys. Rev. Lett. **116**, 211801 (2016).
[32] F. P. An *et al.*, Phys. Rev. Lett. **116**, 061801 (2016).
[33] A. C. Hayes, J. L. Friar, G. T. Garvey, D. Ibeling, G. Jungman, T. Kawano, and R. W. Mills, Phys. Rev. D **92**, 033015 (2015).
[34] D. A. Dwyer and T. J. Langford, Phys. Rev. Lett. **114**, 012502 (2015).
[35] A. A. Sonzogni, T. D. Johnson, and E. A. McCutchan, Phys. Rev. C **91**, 011301 (2015).
[36] A. A. Zakari-Issoufou *et al.*, Phys. Rev. Lett. **115**, 102503 (2015).
[37] O. Tengblad *et al.*, Nucl. Phys. A **503**, 136 (1989).
[38] G. Rudstam *et al.*, At. Data Nucl. Data Tables **45**, 239 (1989).
[39] K. L. Kratz *et al.*, Astron. Astrophys. **125**, 381 (1983).
[40] S. Mughabghab, *Atlas of Neutron Resonances* (Elsevier Science, Amsterdam, 2006).
[41] E. M. Burbidge *et al.*, Rev. Mod. Phys. **29**, 547 (1957).
[42] S. Goriely, Phys. Lett. B **436**, 10 (1998).
[43] R. Surman and J. Engel, Phys. Rev. C **64**, 035801 (2001).
[44] A. Arcones and G. Martinez-Pinedo, Phys. Rev. C **83**, 045809 (2011).
[45] T. Rauscher *et al.*, Atom. Data Nucl. Data Tables **75**, 1 (2000).
[46] J. E. Escher *et al.*, Rev. Mod. Phys. **84**, 353 (2012).
[47] D. R. Slaughter *et al.*, Phys. Lett. B **38**, 22 (1972).
[48] H. Tovedal *et al.*, Nucl. Phys. A **252**, 253 (1975).
[49] F. M. Nuh *et al.*, Nucl. Phys. A **293**, 410 (1977).
[50] S. Raman, B. Fogelberg, J. A. Harvey, R. L. Macklin, P. H. Stelson, A. Schroder, and K. L. Kratz, Phys. Rev. C **28**, 602 (1983).
[51] F. M. Nuh *et al.*, Phys. Lett. B **53**, 435 (1975).
[52] K. L. Kratz *et al.*, Nucl. Phys. A **317**, 335 (1979).
[53] H. Ohm *et al.*, Z. Phys. A **296**, 23 (1980).
[54] C. J. Bischof *et al.*, Phys. Rev. C **15**, 1047 (1977).
[55] G. D. Alkhazov *et al.*, Preprint 1497, Leningrad Nuclear Physics Institute, 1989 (unpublished).
[56] J. P. Omtvedt *et al.*, Z. Phys. A **339**, 349 (1991).
[57] H. Yamamoto *et al.*, Phys. Rev. C **26**, 1215 (1982).
[58] K. L. Kratz *et al.*, Z. Phys. A **312**, 43 (1983).
[59] S. V. Ilyushkin *et al.*, Phys. Rev. C **80**, 054304 (2009).
[60] S. V. Ilyushkin *et al.*, Phys. Rev. C **83**, 014322 (2011).
[61] B. Jonson *et al.*, Proc. 3rd Int. Conf. on Nuclei Far from Stability, CERN Report 76-13, 277, 1976 (unpublished).
[62] R. F. Carlton, R. R. Winters, C. H. Johnson, N. W. Hill, and J. A. Harvey, Phys. Rev. C **38**, 1605 (1988).
[63] M. C. Brady, Ph.D. thesis, Texas A&M University, 1989 (unpublished).
[64] ENDF/B-VII.1, M. B. Chadwick *et al.*, Nucl. Data Sheets **112**, 2887 (2011).
[65] A.-A. Zakari-Issoufou, Ph.D. thesis, University of Nantes (unpublished).
[66] I. Moore *et al.*, Nucl. Instrum. Methods Phys. Res., Sect. B **317**, 208 (2013).
[67] T. Eronen *et al.*, Eur. Phys. J. A **48**, 46 (2012).
[68] S. Agostinelli *et al.*, Nucl. Instrum. Methods Phys. Res., Sect. A **506**, 250 (2003).
[69] J. L. Tain *et al.*, Nucl. Instrum. Methods Phys. Res., Sect. A **774**, 17 (2015).
[70] D. Cano-Ott *et al.*, Nucl. Instrum. Methods Phys. Res., Sect. A **430**, 488 (1999).
[71] J. Agramunt *et al.*, Nucl. Instrum. Methods Phys. Res., Sect. A **807**, 69 (2016).
[72] J. L. Tain *et al.*, Nucl. Instrum. Methods Phys. Res., Sect. A **571**, 719 (2007).
[73] J. L. Tain *et al.*, Nucl. Instrum. Methods Phys. Res., Sect. A **571**, 728 (2007).
[74] D. Cano-Ott *et al.*, Nucl. Instrum. Methods Phys. Res., Sect. A **430**, 333 (1999).
[75] S. Goriely, S. Hilaire, and A. J. Koning, Phys. Rev. C **78**, 064307 (2008).
[76] M.-G. Porquet *et al.*, Eur. Phys. J. A **28**, 153 (2006).
[77] J. Genevey, F. Ibrahim, J. A. Pinston, H. Faust, T. Friedrichs, M. Gross, and S. Oberstedt, Phys. Rev. C **59**, 82 (1999).

[78] See Supplemental Material at http://link.aps.org/supplemental/10.1103/PhysRevC.95.024320 for tables of the β-intensity distribution from this work.
[79] ENSDF Analysis Programs, LOGFT, National Nuclear Data Center, Brookhaven National Laboratory [http://www.nndc.bnl.gov/nndcscr/ensdf_pgm/analysis/logft/].
[80] S. J. Rice, Ph.D. thesis, University of Surrey, 2014 (unpublished).
[81] A. J. Koning *et al.*, J. Korean Phys. Soc. **59**, 1057 (2011).
[82] D. Jordan *et al.*, Phys. Rev. C **87**, 044318 (2013).
[83] B. C. Rasco *et al.*, Phys. Rev. Lett. **117**, 092501 (2016).
[84] A. J. Koning *et al.*, in *Proceedings International Conference on Nuclear Data for Science and Technology*, April 22–27, 2007, Nice, France (EDP Sciences, Paris, 2008), p. 211.
[85] A. J. Koning *et al.*, Nucl. Phys. A **713**, 231 (2003).
[86] P. Möller, B. Pfeiffer, and K. L. Kratz, Phys. Rev. C **67**, 055802 (2003).
[87] A. Spyrou *et al.*, Phys. Rev. Lett. **117**, 142701 (2016).